J. Org. Chem. 2019, 84, 17, 10911−10928 DOI: 10.1021/acs.joc.9b01509

Reverse Turn and Loop Secondary Structures in Stereodefined Cyclic Peptoid Scaffolds

Assunta D'Amato, Giovanni Pierri, Consiglia Tedesco, Giorgio Della Sala, Irene Izzo, Chiara Costabile* and Francesco De Riccardis*

Department of Chemistry and Biology "A. Zambelli", University of Salerno, Via Giovanni Paolo II, 132, Fisciano (SA), 84084, Italy

Keywords: Cyclic peptoids • Secondary structure • Peptidomimetics • Host-guest chemistry

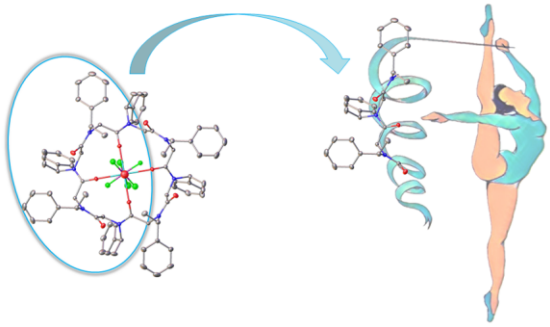

J. Org. Chem. 2019, 84, 17, 10911−10928 DOI: 10.1021/acs.joc.9b01509

ABSTRACT. Controlling the network of intramolecular interactions encoded by *N*α-chiral side chains and the equilibria between *cis*- and *trans*-amide junctions in cyclic peptoid architectures constitutes a significant challenge for the construction of stable reverse turn and loop structures. In this contribution we reveal, with the support of NMR spectroscopy, single crystal X-ray crystallography and DFT calculations, the relevant noncovalent interactions stabilizing tri-, tetra-, hexa-, and octameric cyclic peptoids (as free hosts and host-guest complexes) with strategically positioned *N*-(*S*)-(1-phenylethyl)/*N*-benzyl side chains and how these interactions influence the backbone topological order. With the help of theoretical models and spectroscopic/diffractometric studies we disclose new γ-/β-turn and loop structures present in α-peptoid-based macrocycles and classify them according ϕ, ψ, and ω torsion angles. In our endeavour to characterize emergent secondary structures, we solved the solid state structure of the largest metallated cyclic peptoid ever reported, characterized by an unprecedented alternated *cis*/*trans* amide bonds linkage. Overall, our results indicate that molecules endowed with different elements of asymmetry (central and conformational) provide new architectural elements of facile atroposelective construction and broad conformational stability as minimalist scaffold for novel stereodefined peptidomimetic foldamers and topologically biased libraries necessary for future application of peptoids in all the fields of science.

INTRODUCTION

The control of intramolecular interactions is essential to direct the self-organization of oligomers into defined spatial arrangements and crucial to expedite the transition toward functionally (bio)active structures.[1] The design of malleable amide-based species represents a direct entry into the construction of stable sequence-directed intelligent architectures[2] and factors affecting the oligomers' morphology must be carefully considered.[3] Strategic insertion of bulky/chiral *N*-side chains,[3,4] cyclization,[5] metal ion chelation,[6] and noncovalent interactions[7] (*i.e.*: n→π* interactions,[8] 1,3-allylic strain,[9] Cα−H···O=C and C−F···O=C interactions)[10] determine the conformation of peptoids (*N*-substituted glycine oligomers). Zuckermann was

the first to recognize the effects of *N*α-chiral side chains on the helicity of polyproline type I secondary structures.[4a] Further works[2a,3a,4a,11] confirmed the correlation between side chains stereogenic centers and helix topological arrangement (*S* stereogenic centers induce right-handed helices,[2c,11] *R* configurations form left-handed spirals).[7e] More recently, Cobb and co-workers[10c] demonstrated that fluoroalkyl monomers can be used to influence the $K_{cis/trans}$ of peptoid amide bonds and Faure and Taillefumier offered a novel route to control peptoid amide conformation avoiding aromatic building blocks.[4d,e]

Despite considerable efforts have been devoted to understand the relationships between structural and functional capabilities of linear peptoids, no explicit correlation between side chain configuration, backbone topological order, and conformational stability has ever been established for *cyclic* peptoids.[12]

In this communication we report the preparation of trimeric, tetrameric, hexameric, and octameric cyclic peptoids (and their sodium ion complexes) with strategically positioned *N*-(*S*)-(1-phenylethyl)glycine (*N*spe)/*N*-benzylglycine (*N*pm) residues and describe, for the first time in the cyclic peptoid field, the intricate interplay between side chain configuration, backbone conformational isomerism (based on the amide bonds planar chirality),[2c] and reverse turn/loop topological attributes[13] (Figure 1).

In our endeavour to analyze and classify new peptoid secondary structures, we report the first solid state structure of a cyclic octamer peptoid as a sodium complex (showing an unprecedented alternated *cis/trans* amide backbone arrangement), those of three cyclic peptoids containing chiral side chains,[5d] and that of a unique bicyclic pyrrolopyrazine formed by an unprecedented rearrangement of H-(*N*spe$_3$)-OH during the cyclization reaction. The additive effects of α-chiral aromatic side chains on the conformation of cyclic peptoids have been examined with the help of Density Functional Theory (DFT) calculations, NMR spectroscopy, and X-ray crystallography. The analysis of φ, ψ and ω torsion angles and the surprising conformational homogeneity of some macrocyclic peptoids in solution, as free hosts or sodium ion complexes, showed that weak noncovalent interactions can significantly stabilize secondary structures.

We anticipate that the results presented herein, serve as starting point to better understand the peptoid folding rules and for the design peptoid-based recognition/catalytic sites.

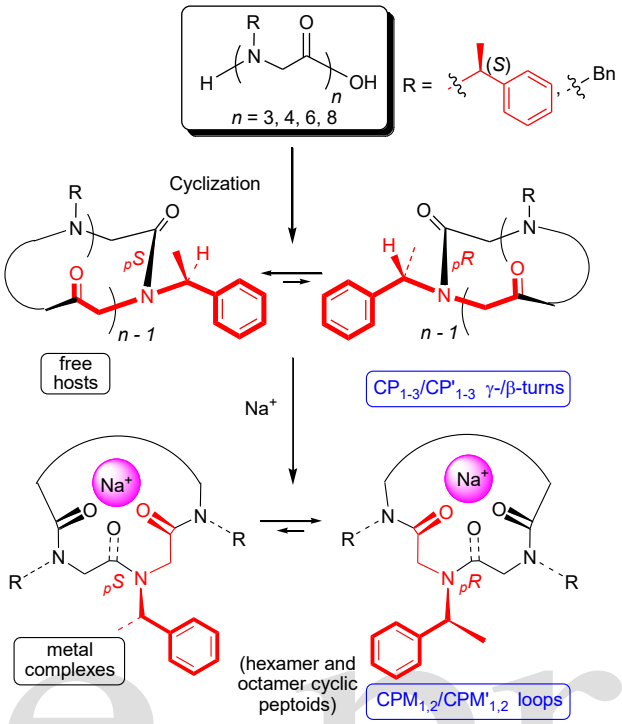

Figure 1. General plan for the synthesis of *N*-(*S*)-(1-phenylethyl)glycine/*N*-benzylglycine-based cyclic α-peptoid oligomers and their sodium complexes as stereodefined reverse turn or loop structures. *N*spe residue evidenced in red.

RESULTS AND DISCUSSION

Synthesis and Structural Properties of Trimeric Cyclic Peptoid Models. Although cyclic peptoids are promising biomimetics, strategies to control their topological order are lacking and formation of mixtures of enantiomorphic or diastereomeric conformational isomers plagues their synthesis and impair their spectroscopic homogeneity.[3b,c] A recently reported method to control their geometric attributes utilized the *N*-benzyl alanine residue as backbone chiral inducer.[7d]

With the aim to simplify the oligomers' synthesis, we selected the classic *N*spe residue as possible chiral inducer and started with the inspection of the simplest possible model prototype: *cyclo*-(*N*spe-*N*pm$_2$).

Preliminary DFT studies showed moderate energy difference for the two possible non-equivalent "crown" conformational isomers *cyclo*-[(*cis*,$_p$*S*)*N*spe-(*cis*,$_p$*S*)*N*pm-(*cis*,$_p$*S*)*N*pm)] (**1**), and *cyclo*-[(*cis*,$_p$*R*)*N*spe-(*cis*,$_p$*R*)*N*pm-(*cis*,$_p$*R*)*N*pm)] (**2**, ΔE = 1.3 kcal mol^{-1} in DMSO, Figure 2a). Lower stability of model **2** was attributed to steric clash between methyl group and carbonyl residue (3.03 Å, Figure 2a and c) and the weaker hydrogen bond between the Cα−H group of the (*S*)-*N*-(1-phenylethyl) side chain and the carbonyl residue[14] (2.39 Å, Figure 2b). Model **1** was stabilized by the sterically interresidue beneficial Ph(Me)NC−H/C=O eclipsing, relieving the 1,3-allylic strain[9] (Figure 2c).

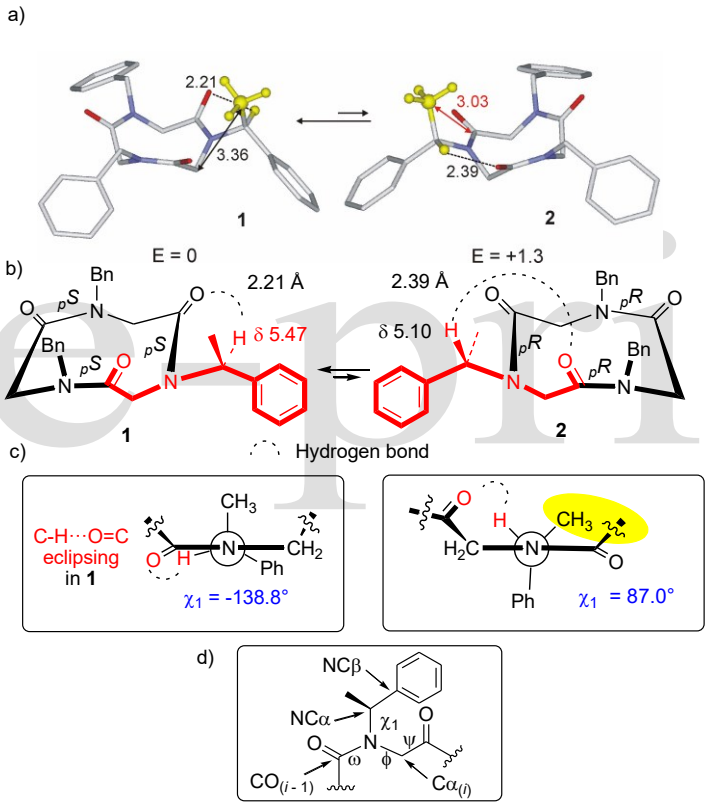

Figure 2. a) Minimum energy structures of **1** and **2** and their respective internal energies calculated in DMSO and expressed in kcal mol^{-1} (see SI for atomic coordinates). Hydrogen atoms have been omitted for clarity (except for the CH–CH$_3$ of the *N*spe residue, in yellow). Atom type: C light grey (yellow for the CH$_3$ residues of *N*spe), N blue, O red. Distances are in Å. b) Schematic structures of conformational isomers **1** and **2**, and key hydrogen bond distances. *N*spe residue is colored in red. c) Newman projections indicating the χ_1 in conformational isomer **1** and **2**. Evidenced in yellow is the steric clash between methyl and carbonyl group. d) Dihedral angles definition for a hypothetical residue *i*:[4d,12a,c] ω [Cα$_{(i-1)}$; CO$_{(i-1)}$; N$_{(i)}$; Cα$_{(i)}$], φ [CO$_{(i-1)}$; N$_{(i)}$; Cα$_{(i)}$; CO$_{(i)}$], ψ [N$_{(i)}$; Cα$_{(i)}$; CO$_{(i)}$; N$_{(i+1)}$], χ_1 [CO$_{(i-1)}$; N$_{(i)}$; NCα; NCβ].

Experimentally, high dilution cyclization of linear H-*N*pm-*N*spe-*N*pm-OH (**3**), in the presence of HATU, yielded the expected "crown"[15] (*i.e.*: *cis*-*cis*-*cis*; *ccc*) conformer **1** and **2**, in a 70:30 ratio, respectively, as an inseparable mixture of conformational isomers in slow equilibrium on the NMR time scale (^{1}H NMR analysis, $(CD_3)_2SO$). The structure of the major conformational isomer was attributed to **1** on the basis of the theoretical studies. Further support came from NMR spectroscopy: the downfield shift of the side chain methine proton chemical shift (δ 5.47 ppm) testified for a shorter hydrogen bond in **1** (compared to δ 5.10 ppm recorded for the same proton in minor atropisomer **2**, Figure 2b).

The energetically favorable inter-residue Ph(Me)NC−H/C=O eclipsing,[9] implicating a $\chi_1 \approx -130°$ torsion angle and due to the *S* side chain configuration in **1**, induced a $_pS$ amide bond planar chirality. Similar values of χ_1 (and consequent $S/_pS$ configurational pairing) have also been evidenced in linear *N*spe$_8$ oligomer ($\chi_1 \approx -120°$),[2c,11] in the X-ray crystal structure of *cyclo*-(*N*spe$_9$) ($\chi_1 \approx -130°$)[4c] and in the right-handed *N*-(*R*)-(1-cyclohexylethyl) linear pentamer *N*rch$_5$ oligomer[7e] (where an enantiomorphous $R/_pR$ configurational pairing is present). Higher energy conformational isomer **2** showed $\chi_1 \approx 90°$ and $S/_pR$ mismatch.

In oligoamides, turn motifs are the most important secondary structures after helices and β-strands. The folding pattern observed in **1** and **2**, typical of trimeric cyclic peptoids,[2c] resembles peptide "open"[13d] γ-turns.[13b,c] The relevant φ and ψ angles for atropisomer **1** fall within the definition of an inverse γ-turn ($\varphi = -79 \pm 40°$, $\psi = 69 \pm 40°$),[13c] the most common form of γ-turn.[16] Torsion angles in **2** evoke "classic" γ-turn (φ from 70 to 95°, ψ from −75 to −45°).[16b] However, lack of hydrogen bonds between residues and, above all, the presence of *cis* amide bonds in cyclic trimeric peptoids require a different classification for these new turn motifs. We suggest the acronym "CP" (from "Cyclic Peptoid") to identify these turns, a subscript number to identify the type and, as in the classic notation, a prime symbol for motifs with opposite torsion angles ("inverse" turns). According to this new notation, cyclic trimeric peptoid **1** and **2** show CP'$_1$ and CP$_1$

type γ-turns, respectively (Figure 3) with $C\alpha_{(i)}$–$C\alpha_{(i+2)}$ distances shorter than 5.5 Å (as typically expected for these kind of turns).[13d]

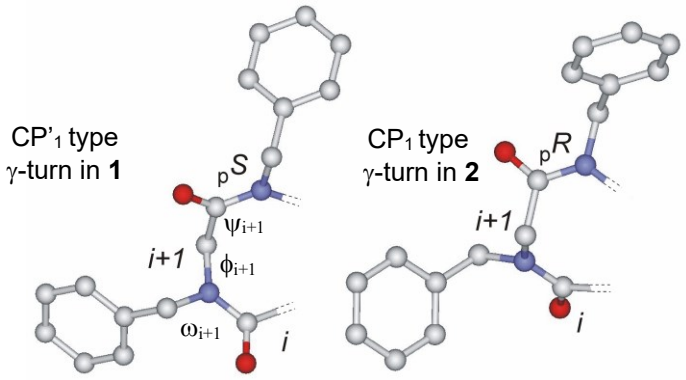

Figure 3. Perspective drawing of cyclotripeptoid **1** and **2** segment structures folded into inverse CP'_1 and classic CP_1 γ-turns in **1** (left) and in **2** (right), respectively. Hydrogen atoms and a fragment of the *N*spe (*i*) residue are omitted for clarity. Atom type: C light grey, N blue, O red.

Idealized ϕ, ψ, and ω torsion angles values (verified by structural data)[2c,5d,7d] and those inferred by theoretical studies, plus $C\alpha_{(i)}$–$C\alpha_{(i+2)}$ distances, have been reported in Table 1.

Table 1. Central residue dihedral angle values, amide bonds planar chirality and $C\alpha_{(i)}$–$C\alpha_{(i+2)}$ distances for CP'_1- and CP_1-type γ-turns in **1** and **2**

Compound	Turn type	ω_{i+1} (planar chirality)	ϕ_{i+1}	ψ_{i+1}	Distance $C\alpha_{(i)}$-$C\alpha_{(i+2)}$ in Å
1	CP'_1	2.0 ($_pS$)	–99.3	94.2	2.97
-	CP'_1[a]	0 ($_pS$)	–95	95	≤5.5
-	Inverse γ[16]	180	–79	69	≤5.5[13d]
2	CP_1	–1.8 ($_pR$)	95.9	–98.3	2.96
-	CP_1[a]	0 ($_pR$)	95	–95	≤5.5
-	Classic γ[16]	180	75	–64	≤5.5[13d]

[a] idealized torsion angles values

With the aim to induce the formation of a single conformational isomer, we attempted the synthesis of prototypes with two and three chiral residues (*cyclo*-(*N*spe$_2$-*N*pm), **4**, and *cyclo*-(*N*spe$_3$), **5**, Figure 4). However, cyclization in the usual conditions of linear H-*N*pm-*N*spe$_2$-OH (**6**) and H-*N*spe$_3$-OH (**7**), gave

rearranged dehydrated congeners **8** and **9**, in 25 and 26% yield, respectively, and no trace of the expected **4** and **5** (Figure 4).[17]

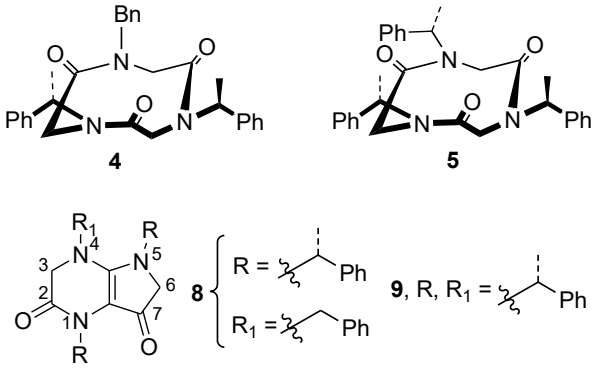

Figure 4. Expected (**4** and **5**) and unexpected (**8** and **9**) products in the cyclization of linear trimeric H-*N*pm-*N*spe$_2$-OH (**6**), and H-*N*spe$_3$-OH (**7**).

The structure of the unprecedented 3,4,5,6-tetrahydro-1H-pyrrolo[2,3-b]pyrazine-2,7-dione heterocyclic nucleus[17] was inferred by accurate analysis of their one- and two-dimensional NMR spectra (see SI). It was attributed to an exceptional double intramolecular segment coupling linking the oligomers termini to the central amide junction *via* formation of an oxazolonium ion intermediate[18,19] (**11**), *N*-terminal aminolysis (from **11** to **12**) and pyrrole ring closure (to form hypothetical immonium **14**, Scheme 1).

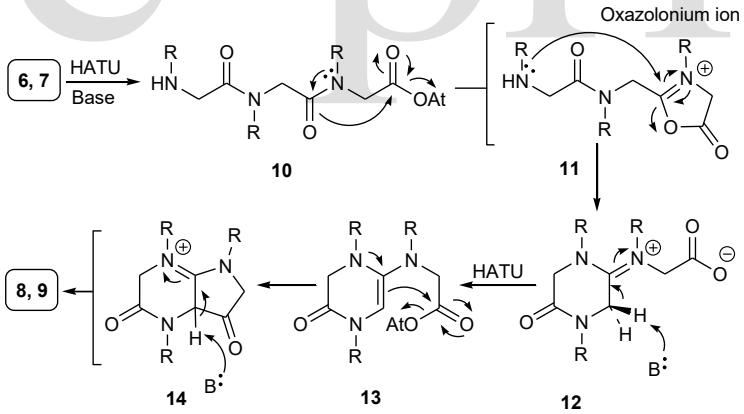

Scheme 1. Suggested mechanism for the formation of pyrrolopyrazine **8** and **9** from high dilution condensation of H-*N*pm-*N*spe$_2$-OH (**6**) and H-*N*spe$_3$-OH (**7**). At = 7-azabenzotriazole; R = benzyl or (*S*)-*N*-(1-phenylethyl) side chain.

Formation of bicyclic products starting from linear tripeptoids with three *N*spe residues is thermodynamically reasonable if we compare the free energy of formation of cyclopeptoid **5** (–7.5 kcal mol^{-1}) and bicyclic **9** (–15.1 kcal mol^{-1}, as predicted by DFT calculations) and take into account the entropically

favorable development of two water molecules for the formation of pyrrolopyrazine **9** (instead of one, as in **5**).

Recrystallization trials on a microcrystalline sample of rearranged **9** provided single crystals suitable for X-ray diffraction. X-ray analysis confirmed the formation of a pyrrolopyrazine nucleus and revealed the presence of a hydroxyl group on C3, due to autoxidation processes[20] (**15**, Figure 5).

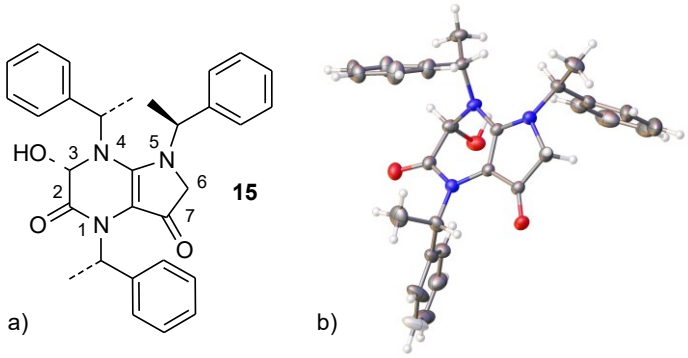

Figure 5. Structure ORTEP drawing of bicyclic compound **15**. Ellipsoids are drawn at 20% probability level. Atom type: C grey, N blue, O red, H white.

The intermolecular hydrogen bonding between C-7 carbonyl oxygen and hydroxyl group (OH···O 2.677 Å, O-H···O 169.3°) facilitates the crystallization of **15** giving rise to a left-handed helix through the crystallographic 2_1 screw axis parallel to the shortest cell axis (*i.e. a* axis).

Synthesis and Structural Properties of Tetrameric Cyclic Peptoid Models. Cyclic *cis-trans-cis-trans* (*ctct*) tetrapeptoids are gifted minimalist scaffolds for the generation of reverse turn "conformational templates".[7d,21] DFT studies on tetrapeptoids with a single *N*α-chiral side chain indicated a small energy difference between the lowest energy *cyclo*-[(*cis*,$_p$*R*)*N*pm-(*trans*,$_p$*R*)*N*pm-(*cis*,$_p$*S*)*N*spe-(*trans*,$_p$*S*)*N*pm], **16** (showing a favorable *S*/$_p$*S* configurational pairing due to a reduced allylic strain, χ_1 = -106.4°), and the higher energy *cyclo*-[(*cis*,$_p$*S*)*N*pm-(*trans*,$_p$*S*)*N*pm-(*cis*,$_p$*R*)*N*spe-(*trans*,$_p$*R*)*N*pm], **17** (displaying a *S*/$_p$*R* configurational mismatch originated by the unfavorable χ_1 = 85.6°, ΔE = 1.3 kcal mol^{-1}, Figure 6).

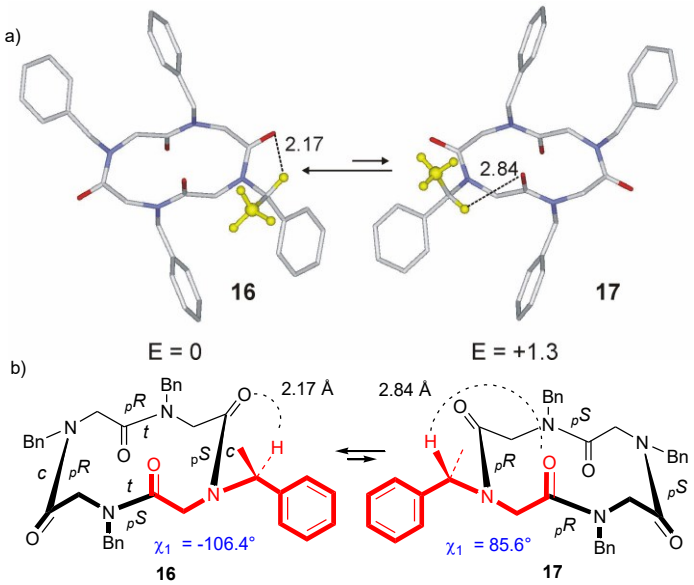

Figure 6. a) Minimum energy and schematic structures of conformational diastereoisomers **16** and **17** and their respective internal energies calculated in chloroform and expressed in kcal mol^{-1}. Hydrogen atoms have been omitted for clarity except for the $CHCH_3$ of the *N*spe residue (in yellow). Atom type: C light grey (yellow for the CH_3 residues of *N*spe), N blue, O red (see SI for atomic coordinates). Distances are in Å. b) Schematic structures of conformational diastereoisomers **16** and **17** with, in red, the *N*spe residue; *c* = *cis*; *t* = *trans*.

Cyclization of the H-*N*pm$_2$-*N*spe-*N*pm-OH linear sequence (**18**) yielded an inseparable mixture of the expected conformational isomers **16** and **17** in a 85:15 ratio, respectively (^{1}H NMR analysis), in a slow equilibrium on the NMR time scale. The downfield shift of the side chain methine proton observed for the major conformational isomer (δ 5.92, due to the short C-H···O=C distance) confirmed **16** as the most stable conformer in the mixture. The relatively high values (>5.00 ppm) found for the Ph(Me)C-H protons in both **16** and **17**, attested the presence of the *N*α-chiral side chains on *cisoid* amide bonds.[4a,12b]

Crystallization trials of cyclooligomers mixture **16**/**17** afforded single crystals suitable for X-ray diffraction analysis by dissolution in hot dichloromethane. Structural analysis showed that only the lowest energy cyclo-oligomer **16** crystallized, confirming the structural hypothesis based on DFT and NMR studies (Figure 7).

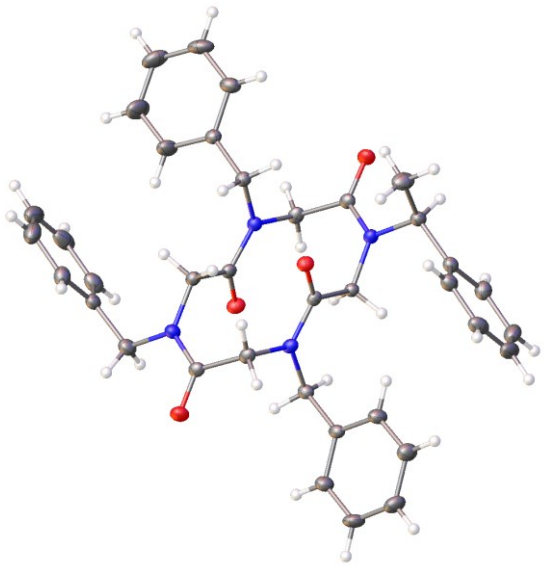

Figure 7. ORTEP drawing of compound **16**. Ellipsoids are drawn at 20% probability level. Atom type: C grey, N blue, O red, H white.

The secondary structure present in tetrameric cyclopeptoids (Figure 7 and 8) is reminiscent of type VI β-turn (characterized by the presence of a *cis*-proline at the $i + 2$ residue).[13] However, for the large deviations from the canonical values,[16] the turn motifs in **16** and **17** are better described as type CP_2 and CP'_2 β-turns (formally belonging to non-classified c).

It is interesting to note that for the peculiar symmetry properties of the *ctct* oligoamide framework (which, in the absence of a chiral side chain, would show an inversion center),[22] CP_2 and CP'_2 turns are present in both the halves of tetramers **16** and **17** (blue and black part of each molecule, Figure 8a).

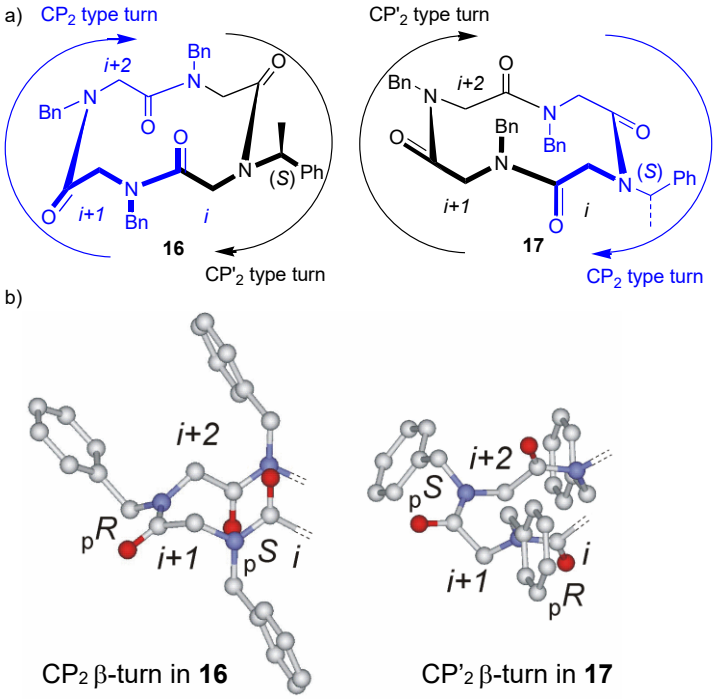

Figure 8. a) Schematic structures of conformational diastereoisomers depicting type CP_2 and CP'_2 β-turns present in **16** and **17**. The arrows point toward the CO→N direction. b) Models of CP_2 and CP'_2 β-turns extracted from the minimum energy structures of **16** and **17**, respectively. Hydrogen atoms are omitted for clarity. Residue *i* and *i* +3 are partially omitted for clarity. Atom type: C light grey, N blue, O red.

ϕ, ψ, and ω torsion angles of **16** and **17** are reported in Table 2.[2c,5d,7d] The table also includes the values of type VIb β-turn (the closest to the CP'_2 turn) and the $C\alpha_{(i)}$–$C\alpha_{(i+3)}$ distances (always shorter than 7.0 Å, as typically expected for classic β-turns).[13a]

Table 2. Central residues dihedral angle values, amide bonds planar chirality and $C\alpha_{(i)}$−$C\alpha_{(i+3)}$ distances for type CP_2 and CP'_2 *tct* β-turns in **16**, **17**, and **19**

Compound	β-Turn type	ω_{i+1} (planar chirality)	ϕ_{i+1}	ψ_{i+1}	ω_{i+2} (planar chirality)	ϕ_{i+2}	ψ_{i+2}	Distance $C\alpha_{(i)}$-$C\alpha_{(i+3)}$ in Å
16[a]	CP_2	–170.7 ($_pS$) (–169.5)	118.8 (118.9)	–65.8 (–69.4)	–6.6 ($_pR$) (0.8)	93.8 (91.6)	–169.9 (–172.4)	2.93 (2.89)
17	CP_2	–170.4 ($_pS$)	119.6	–59.2	–13.8 ($_pR$)	100.34	–171.7	2.91
19[a]	CP_2	–170.4 ($_pS$) (–171.1)	121.3 (118.4)	–67.4 (–60.0)	–2.7 ($_pR$) (–13.4)	93.0 (99.6)	–173.0 (–170.8)	2.93 (2.87)
-	CP_2[b]	180 ($_pS$)	120	–65	0 ($_pR$)	95	–170	≤ 7
16[a]	CP'_2	170.0 ($_pR$) (170.4)	–119.6 (–121.5)	65.3 (63.4)	5.4 ($_pS$) (7.2)	–91.0 (–95.1)	171.8 (171.2)	2.93 (2.86)
17	CP'_2	169.0 ($_pR$)	–119.1	64.2	7.4 ($_pS$)	–95.1	170.0	2.94
19[a]	CP'_2	169.4 ($_pR$) (171.8)	–119.0 (–120.9)	64.3 (63.4)	5.5 ($_pS$) (6.5)	–91.7 (–93.8)	171.5 (170.4)	2.91 (2.83)
-	CP'_2[b]	180 ($_pR$)	–120	65	0 ($_pS$)	–95	170	≤ 7
-	VIb[16]	180	–135	135	0	–75	160	≤ 7[13a]

[a] in parenthesis data from the X-ray crystal structures

[b] idealized torsion angles values

In order to evaluate the effect of multiple substitution of bulky chiral groups on the conformational stability of tetrameric scaffold, we embarked in the synthesis of *cyclo*-[(*N*spe-*N*pm)$_2$] and *cyclo*-(*N*spe$_4$).

Preliminary conformational search on *cyclo*-[(*N*spe-*N*pm)$_2$] and subsequent DFT calculations predicted the formation of an atropisomer with both the *N*-(*S*)-(1-phenylethyl) side chains on *cis*-amide bonds (*i.e.*: *cyclo*-[(*cis*,$_p$*R*)*N*spe-(*trans*,$_p$*R*)*N*pm-(*cis*,$_p$*S*)*N*spe-(*trans*,$_p$*S*)*N*pm], **19**, ΔE = 0.0 kcal mol^{-1}). Bulky chiral side chains on *trans* positions raised the energy of the hypothetical **20**, to ΔE = 3.8 kcal mol^{-1} (Figure 9a).

Successful experimental head-to-tail cyclization of linear precursor H-*N*spe-*N*pm-*N*spe-*N*pm-OH (**21**) yielded the asymmetric cyclopeptoid *ctct*-**19** as the only revealed conformational isomer (^{1}H NMR analysis, Figure 9b). Its structure was confirmed by the relatively high chemical shift values of the non-equivalent

methine protons linked to *cis* peptoid junctions (δ 5.86 and 5.38 ppm)[4a,12b] and the presence of the two benzyl groups on *transoid* junctions (attested by the small Δδ values detected for the diastereotopic methylene protons: 0.22 and (

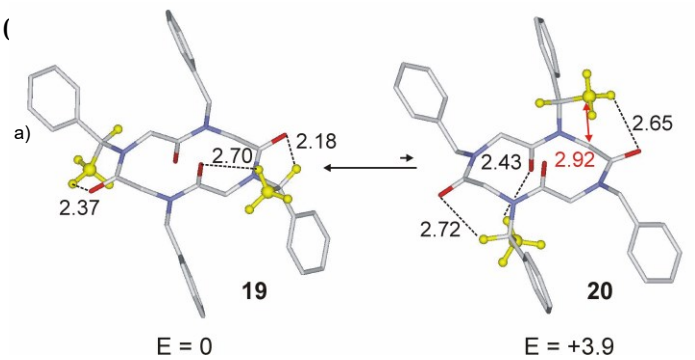

Figure 9. a) Minimum energy structures and their respective internal energies calculated in chloroform and expressed in kcal mol^{-1}; distances in black report the favorable hydrogen bonds, in red the unfavorable C-C distance. Hydrogen atoms have been omitted for clarity except some in the *N*spe residue (in yellow). Atom type: C light grey (yellow for the CH_3 residues of *N*spe), N blue, O red (see SI for atomic coordinates). Distances are in Å. b) Schematic structures of conformational isomers **19** and **20** with, in red, the chiral residues. The arrow in **19** (following the CO→N direction) depicts CP_2 type β-turn.

With the aim to confirm the structural hypothesis based on DFT and NMR studies, we attempted the crystallization of compound **19**. To our delight, recrystallization from a solution of chloroform/toluene (2:1) afforded single crystals suitable for the X-ray diffraction studies (Figure 10).

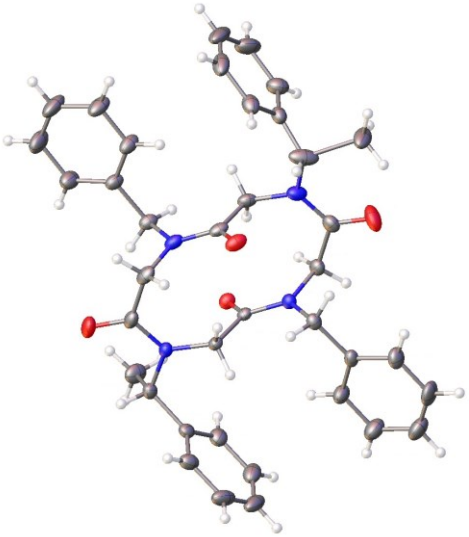

Figure 10. ORTEP drawing of compound **19**. Ellipsoids are drawn at 20% probability level. For clarity only one possible position for disordered atoms is displayed. Atom type: C grey, N blue, O red, H white.

Compound **19** crystallizes in space group $P2_1$ with a *ctct* tetralactam core geometry and overall rectangular shape of the peptoid backbone in agreement with DFT model and NMR studies.

Close proximity of bulky residues (in the case of easily assembled linear H-*N*spe$_4$-OH, **22**) prevented cyclization of the tetrameric oligomer, yielding a complex mixture of inseparable oligopeptoids, instead of the expected *cyclo*-(*N*spe$_4$), **23**.

Synthesis and Structural Properties of Hexameric Cyclic Peptoid Models. While trimeric and tetrameric cyclic peptoids display relatively rigid scaffolds ($\Delta G^{\ddagger}$ for the ring inversion > 20 kcal mol^{-1}),[2c,23] hexameric and octameric macrocycles often show multiple isoenergetic conformations in slow equilibrium on the NMR time scale ($\Delta G^{\ddagger}$ ~ 14-16 kcal mol^{-1}).[2c,d,3,5c,7d,22,24] Given the intrinsic instability of larger cyclohexapeptoids, we decided to probe the conformational stability of three different structures showing a single, three alternated, and six chiral side chains in the sequence. If, on one side, cyclization of the linear oligomer with one chiral side chain (H-*N*pm$_4$-*N*spe-*N*pm-OH, **24**) induced the formation of cyclooligomer

27 as a complex mixture of multiple species in slow equilibrium on the NMR time scale (Figure 11, see NMR spectra in the SI), head-to-tail condensation of oligomers with multiple *N*α-chiral side chains (H-(*N*spe-*N*pm)$_3$-OH, **25** and H-*N*spe$_6$-OH, **26**) yielded *cctcct*-**28** (or *cctcct*-**29**, as a possible alternative conformational isomer) and *cctcct*-**30** as a major conformationally homogeneous species (Figure 11 and NMR spectra in the SI).

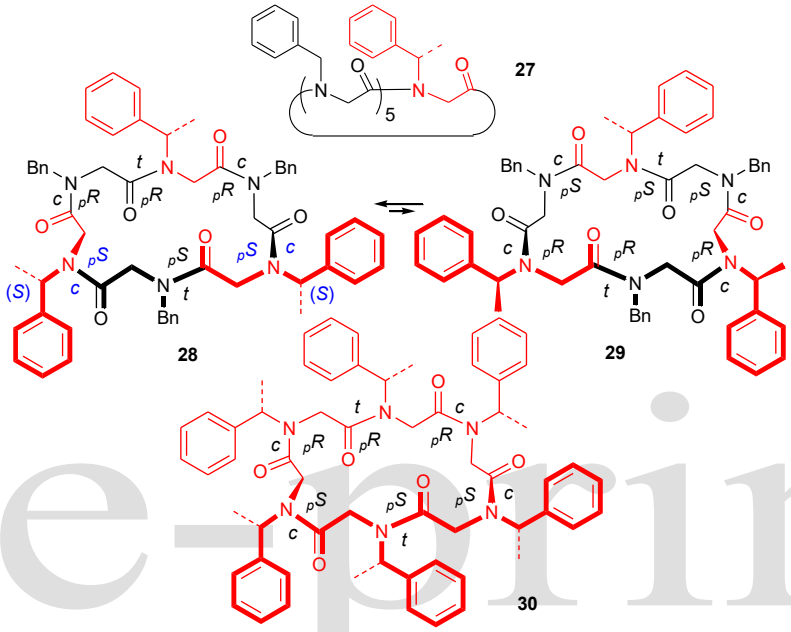

Figure 11. Schematic structures of cyclic hexameric peptoids **27-30** with, in red, the *N*spe chiral residues.

The *cctcct* arrangement of **28** (or **29**) was suggested by the accurate analysis of its ^{1}H NMR spectrum. The presence of two *N*-1-(*S*)-(1-phenylethyl) and two *N*-benzyl side chains on *cis* amide bonds was inferred by the resonance of the (*S*)-(1-phenylethyl) Cα−H groups at δ 5.98/5.74, and the large difference of the benzyl groups' diastereotopic protons (Δδ 1.87/1.48 ppm).[12b] The two remaining chiral and benzyl side chains were located on the two *transoid* junctions (δ 4.78 for the Cα−H group and Δδ 0.35 ppm for the diastereotopic protons of the benzyl group).[12b]

Support for the formation of conformer **28** (*cyclo*-[(*cis*,$_p$*R*)*N*pm-(*trans*,$_p$*R*)*N*spe-(*cis*,$_p$*R*)*N*pm-(*cis*,$_p$*S*)*N*spe-(*trans*,$_p$*S*)*N*pm-(*cis*,$_p$*S*)*N*spe], with the matching *cis*-(*S*,$_p$*S*) configurations, evidenced in blue color in Figure

11) came from DFT calculations[25] (**29**: ΔE = 3.6 kcal mol^{-1}, Figure 12). Formation of key hydrogen bonds between side chains methine groups on *cis* amide bonds and adjacent carbonyl groups (C−H···O=C distance: 2.19 and 2.33 Å, Figure 12) increased the stability of the former structure.

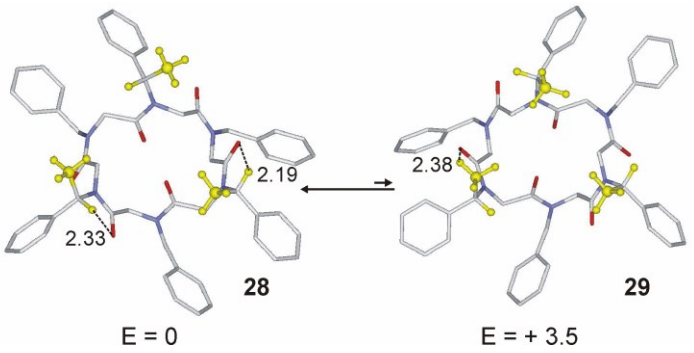

Figure 12. Minimum energy structures of **28** and **29** and their respective internal energies calculated in chloroform and expressed in kcal mol^{-1} with reported hydrogen bonds as dotted lines (and atomic distances). Hydrogen atoms have been omitted for clarity except some in the *N*spe residue (in yellow). Atom type: C light grey (yellow for the CH_3 residues of *N*spe), N light blue, O red (see SI for atomic coordinates). Distances are in Å.

As revealed by Kirshenbaum and co-workers (studying the solid state structure of *cyclo*-[(*N*me-*N*pm)$_3$] model),[5c] the *cctcct*-hexapeptoid backbone is morphologically similar to type I (and III) β-turns. However, the large differences in the torsion angles plus the presence of two *cis* bonds in the peptoid turn motif, suggested the use of a different type of classification reported in Figure 13 (CP_3 and CP'_3). In terms of torsion angles, CP_3 and CP'_3 type turn motifs are more similar to the right handed poly-proline I (PPI) helix ($\varphi = -75°$, $\psi = 160°$) and the left handed PPI helix ($\varphi = 75°$, $\psi = -160°$), respectively. The main difference between CP_3 and CP'_3 and PPI models is the planar chirality of the amide bond (which is opposite in the peptoid and peptide models, as evidenced in Table 3). It is interesting to note that in larger cyclic peptoids (with six or more residues), where the ring strain is lower, the ϕ and ψ torsion angles ($\varphi \approx 70°$ and $-70°$ and $\psi \approx 180°$ and $-180°$) are similar to those reported for most published peptoid structures.[12d]

ϕ, ψ, and ω dihedral angles values and the $C\alpha_{(i)}$−$C\alpha_{(i+3)}$ distances for CP_3 and CP'_3 β-turns for cyclic hexameric peptoids **28** and **30** are reported in Table 3.

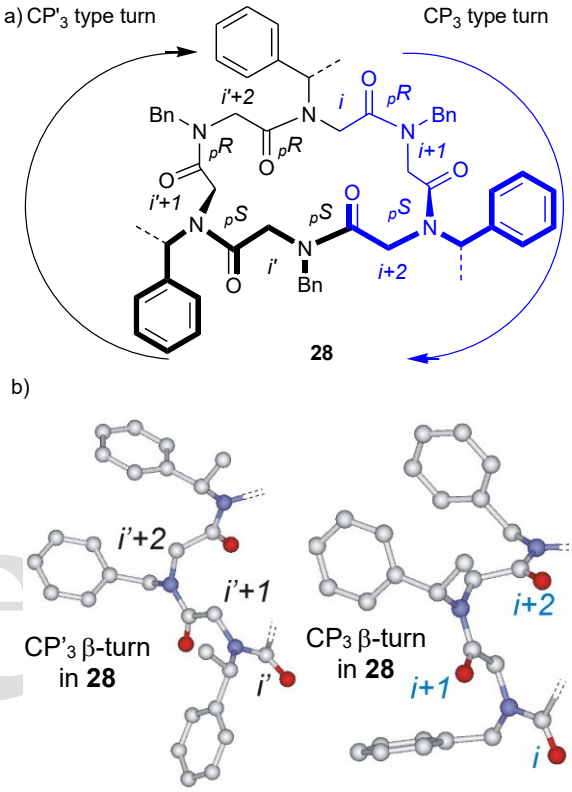

Figure 13. a) Schematic structures of **28** depicting type CP'_3 (in black) and CP_3 (in blue) *cct* β-turns with arrows pointing towards the CO→N direction. b) Models of type CP'_3 (left) and CP_3 (right) *cct* turns present in the minimum energy structures of **28**. Hydrogen atoms are omitted for clarity. Atom type: C light grey, N blue, O red.

Table 3. Central residues dihedral angles values, amide bonds planar chirality and $C\alpha_{(i)}$−$C\alpha_{(i+3)}$ distances for type CP_3 and CP'_3 turns in **28**/**30** and PPI helix

Compound	β-Turn type/helix	ω_{i+1} (planar chirality)	ϕ_{i+1}	ψ_{i+1}	ω_{i+2} (planar chirality)	ϕ_{i+2}	ψ_{i+2}	Distance $C\alpha_{(i)}$-$C\alpha_{(i+3)}$ in Å
28	CP_3	12.4 ($_pR$)	−74.0	176.7	−7.6 ($_pS$)	−69.4	168.6	5.35
30[a]	CP_3	18.4 ($_pR$)	−75.8	167.6	−0.2 ($_pS$)	−79.1	−179.2	5.41
-	CP_3[b]	0 ($_pR$)	−75	175	0 ($_pS$)	−75	175	≤ 7
-	Right handed PPI helix	0 ($_pS$)	−75	160	-	-	-	
28	CP'_3	−16.1 ($_pS$)	77.9	−176.4	5.7 ($_pR$)	74.6	−170.4	5.35
30[a]	CP'_3	−19.9 ($_pS$)	75.7	−174.7	−2.0 ($_pR$)	78.6	−159.9	5.41
-	CP'_3[b]	0 ($_pS$)	75	−175	0 ($_pR$)	75	−175	≤ 7
-	Left handed PPI helix	0 ($_pR$)	75	−160	-	-	-	

[a] data from X-ray crystal structure

[b] idealized values

The *cctcct*-peptoid bond arrangement present in cyclooligomer **30** was suggested by the presence of four *N*-1-(*S*)-(1-phenylethyl) side chains on *cis* amide bonds (δ 6.05, 5.95, 5.72, and 5.30 for the Cα−H groups) and two *N*α-chiral side chains on *trans* amide bonds (δ 4.83 and 4.72). It is interesting to note that for its specific symmetry properties, configurational inversion of all the amide bonds gives back the same structure (*i.e.*: *cyclo*-[(*cis*,$_p$*R*)*N*spe-(*trans*,$_p$*R*)*N*spe-(*cis*,$_p$*R*)*N*spe-(*cis*,$_p$*S*)*N*spe-(*trans*,$_p$*S*)*N*spe-(*cis*,$_p$*S*)*N*spe], Figure 11) and therefore just one *cctcct*-conformational isomer is possible for this macrocyclic species.

Accurate X-ray diffraction studies confirmed the structure and torsion angle values for type CP_3 and CP'_3 turns (Figure 14).[26]

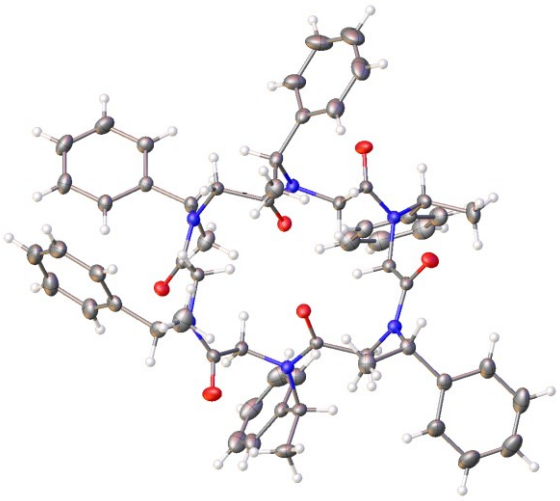

Figure 14. ORTEP drawing of conformational isomer **30**. Ellipsoids are drawn at 20% probability level. Atom type: C grey, N blue, O red, H white.

Macrocycles **28** and **30** add up to the small group of conformationally stable cyclic hexamer peptoids[12a] (on the NMR time scale) and constitute the only known examples of rigid (non-*N*-arylated and non-complexed) hexameric cyclopeptoids with stereodefined backbone conformations.

Synthesis and Structural Properties of Octameric Cyclic Models. Cyclic octamer peptoids are the largest members of the cyclopeptoid family showing homogeneous conformations in solution.[2e,3b,c,22,24] With the aim to evaluate the stereoelectronic and topological influence of the *N*-1-(*S*)-(1-phenylethyl) side chain on this rare class of peptidomimetics, we have synthesized three linear octamer peptoid precursors. The first one contained a single chiral side chain (H-*N*pm$_6$-*N*spe-*N*pm-OH, **31**), the second one showed a set of paired *N*spe$_2$/*N*pm$_2$ residues matching the *ccttcctt* amide bond sequence found in most of the conformationally rigid cyclic octamer peptoids[2c] (H-*N*pm-*N*spe$_2$-*N*pm$_2$-*N*spe$_2$-*N*pm-OH, **32**), and the last one displayed eight chiral amino acid residues (H-*N*spe$_8$-OH, **33**) in the primary sequence.

While high dilution macrocyclization of **31** and **32**, produced conformationally heterogeneous macrocycles **34** and **35** (Figure 15), cyclization of homooligomer **33** showed the presence of a two-fold symmetric species (^{1}H NMR analysis, $C_6D_5CD_3$, 62% of the conformational isomers mixture, see SI) with four side

chains located on *cisoid* bonds (δ 6.14/5.47 for the Cα−H groups) and four positioned on *transoid* junctions (δ 4.40/4.22) suggesting the formation of one of the two possible inequivalent C_2-symmetric[22] *ccttcctt* conformational isomers **36** or **37**.

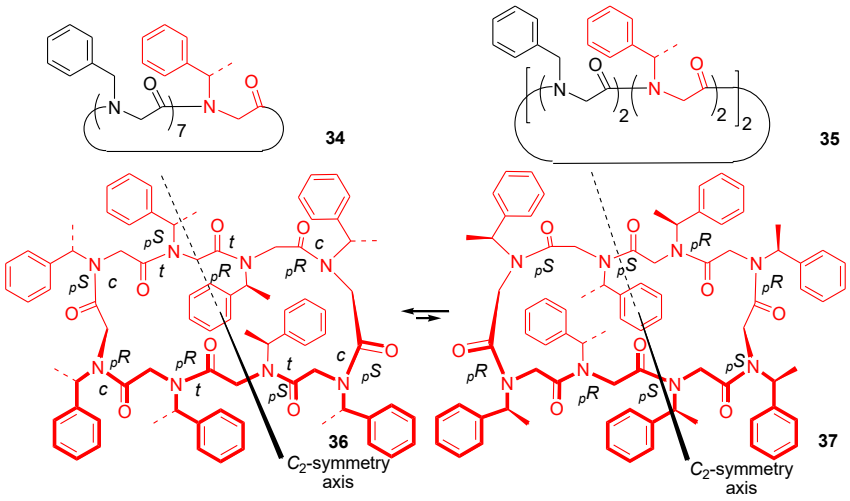

Figure 15. Schematic structures of the synthesized cyclic octameric peptoids **34**, **35**, and conformational isomer **36** or **37** with, in red, residues with chiral side chain.

Differently from the lower homologue **30**, the concurrent inversion of amide bonds generates two inequivalent species: conformational isomers **36** and **37**. The analysis of the NMR spectra evidenced the presence of a major species. In order to establish the identity of the most stable conformational isomer, detailed DFT studies were performed. Multiple unfavourable steric interactions between methyl and carbonyl groups were found in *cyclo*-{[(*cis*,$_p$*S*)*N*spe-(*cis*,$_p$*R*)*N*spe-(*trans*,$_p$*R*)*N*spe-(*trans*,$_p$*S*)*N*spe]$_2$}, **37**, to ΔE = 2.6 kcal mol^{-1} (Figure 16) and pointed towards the formation of *cyclo*-{[(*cis*,$_p$*R*)*N*spe-(*cis*,$_p$*S*)*N*spe-(*trans*,$_p$*S*)*N*spe-(*trans*,$_p$*R*)*N*spe]$_2$}, **36**.[27]

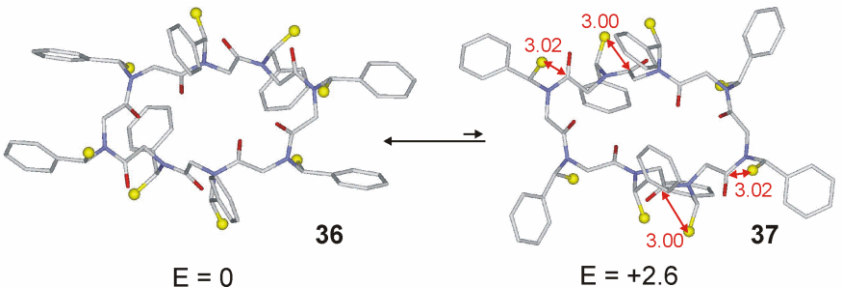

Figure 16. Minimum energy structures of **36** and **37** and their respective internal energies calculated in chloroform and expressed in kcal mol^{-1}. The unfavorable steric interactions present in conformational isomer **37** evidenced in red. Hydrogen atoms have been omitted for clarity. Atom type: C light grey (yellow for the CH_3 residues of *N*spe), N light blue, O red (see SI for atomic coordinates). Distances are in Å.

C$_2$-symmetric macrocyclic peptoid **36** shows the same ϕ, ψ, and ω dihedral angles in both the β-turns present in the oligomer (φ_{i+1} = −78.8°, ψ_{i+1} = −173.7°; φ_{i+2} = −69.2°, ψ_{i+2} = 164.2°), compatible with type CP_3 β-turn (Figure 17 and Table 4).[5c] The enantiomorphic type CP'_3 β-turn (with opposite torsion angles/amide bonds planar chirality) would be observable in a hypothetical cyclooctamer with *N*-(*R*)-(1-phenylethyl) side chains (*i.e.*: *ent*-**36**).

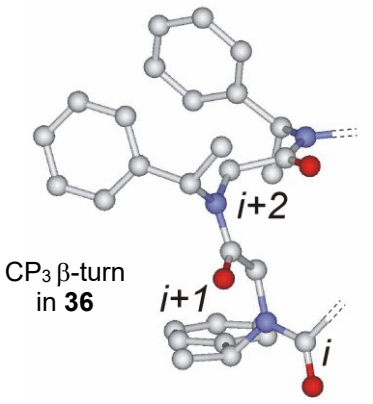

Figure 17. Model of type CP_3 turn in the minimum energy structures of *C*$_2$-symmetric **36**. Hydrogen atoms are omitted for clarity. Atom type: C light grey, N blue, O red.

Table 4. Central residues dihedral angles values, amide bonds planar chirality and $C\alpha_{(i)}$–$C\alpha_{(i+3)}$ distances for type CP_3 *cct* turn in **36**

Compound	β-Turn type	ω_{i+1} (planar chirality)	ϕ_{i+1}	ψ_{i+1}	ω_{i+2} (planar chirality)	ϕ_{i+2}	ψ_{i+2}	Distance $C\alpha_{(i)}$-$C\alpha_{(i+3)}$ in Å
36	CP_3	–4.8 ($_pR$)	–78.8	–173.7	–9.1 ($_pS$)	–69.2	164.2	5.28

Sodium Complexation Studies on Hexameric Cyclic Peptoid Models. Addition of metal ions to solutions of larger cyclic peptoids promotes the formation of all-*trans* 1:1[3b] host/guest complexes.[2c,7d,12b,f,22,28] Stepwise quantitative additions of sodium tetrakis[3,5-bis(trifluoromethyl)phenyl]borate (NaTFPB) to $CDCl_3$ solutions of cyclohexamer **28** and **30** led to metallated species in slow equilibrium with the respective free hosts on the NMR time scale (see titration experiments in Figures S2 and S3). Formation of all-*trans* three-fold symmetric [**28**·Na]$^+$ and [**30**·Na]$^+$ species (log K_{ass} = 4.4, $\Delta G°$ = –6.0 kcal mol^{-1}, and log K_{ass} = 4.3, $\Delta G°$ = –5.9 kcal mol^{-1}, respectively, calculated by ^{1}H NMR, 3.0 mM host/guest solutions in $CDCl_3$, see SI), was attested by the simplification of the ^{1}H NMR spectra of the complexes (Figure 18), methine protons upfield shift (quartet signals at δ < 5.01) and low $\Delta\delta$ values for diastereotopic benzyl protons ($\Delta\delta$ < 0.27).

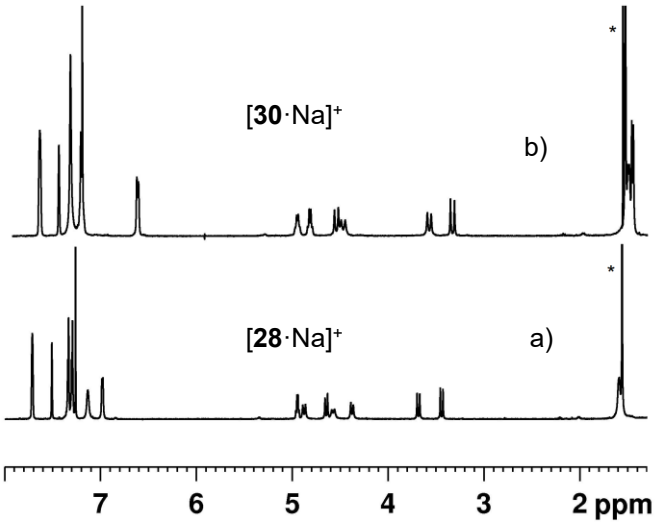

Figure 18. ^{1}H NMR spectra of a) [**28**·Na]$^+$ and b) [**30**·Na]$^+$ complexes as NaTFPB salts in $CDCl_3$ (600 MHz, 8.0–1.3 ppm expansion). Water impurity denoted with *.

Metallation of **28**, in principle, yields two possible non-equivalent all-*trans* C_3-symmetric conformational isomers: [*cyclo*-[(*trans*,$_p$*R*)*N*spe-(*trans*,$_p$*S*)*N*pm]$_2$·Na]$^+$ and [*cyclo*-[(*trans*,$_p$*S*)*N*spe-(*trans*,$_p$*R*)*N*pm]$_2$·Na]$^+$, [**28a**·Na]$^+$ and [**28b**·Na]$^+$, respectively (Figure 19a).

Theoretical (DFT) studies indicated [**28b**·Na]$^+$ as the higher energy atropisomer for the repulsive steric interactions between the methyl side chains (in yellow in Figure 19b) and intra-annular methylene groups (ΔE = 14.1 kcal mol^{-1}). It is interesting to note that while in *cis* peptoid junctions, *S* side chains induce $_p$*S* amide configurations (as reported for most of the cyclic species as free hosts and for all the studied linear peptoids), in *trans* amide bonds this configuration stabilizes $_p$*R* planar chirality.

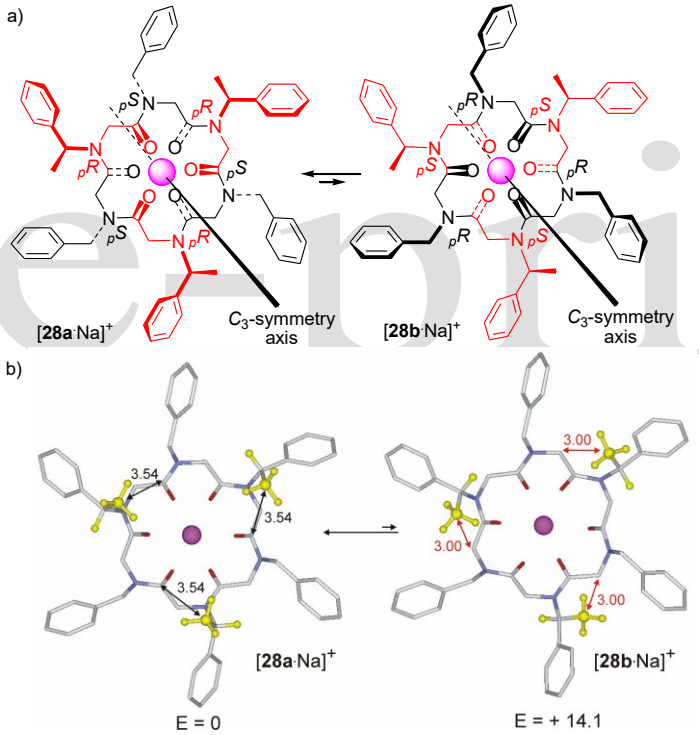

Figure 19. a) Schematic structures of all-*trans* conformational diastereoisomers [**28a**·Na]$^+$/[**28b**·Na]$^+$ with, in red, the chiral residues (Na$^+$ as the magenta sphere); b) Minimum energy structures and their respective internal energies calculated in chloroform and expressed in kcal mol^{-1}. Hydrogen atoms have been omitted for clarity except for selected H residues of *N*spe (in yellow). Atom type: C light grey (yellow for the CH_3 of *N*spe), N blue, O red, Na magenta (see SI for atomic coordinates). Distances are in Å.

For symmetry reason, metalation of cyclohomooligomer **30** forms a *single* all-*trans* atropisomer: [(*cyclo*-[(*trans*,$_{p}$*R*)*N*spe-(*trans*,$_{p}$*S*)*N*spe]$_2$·Na]$^+$, [**30a**·Na]$^+$, illustrated in the minimum energy DFT structure (Figure 20). Configurational inversion of all the amide bonds, in fact, does not change the structure.

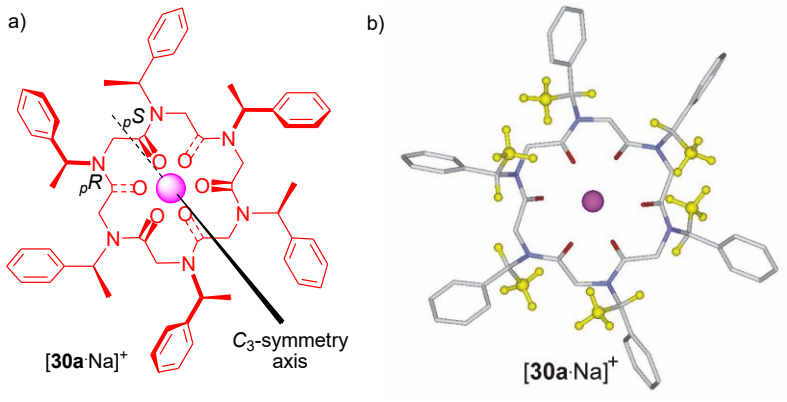

Figure 20. a) Schematic structures of [**30a**·Na]$^+$ with, in red, the chiral residues (Na$^+$ as the magenta sphere); b) Minimum energy structure calculated in chloroform. Hydrogen atoms have been omitted for clarity except for the H residues of *N*spe (in yellow). Atom type: C light grey (yellow for the CH_3 residues of *N*spe), N light blue, O red, Na$^+$ magenta (see SI for atomic coordinates).

The pleated *ttt* arrangement present in both [**28a**·Na]$^+$ and [**30a**·Na]$^+$ features a loop structure (the distance between the C$\alpha_{(i)}$ and the C$\alpha_{(i+3)}$ is larger than 7.0 Å). We suggest to name this folding, typical of hexameric metallated cyclic peptoids, as "CPM$_1$ loop" (Figure 21, M stands for Metal). CPM$_1$ loop's torsion angles are similar to the left handed poly-proline II (PPII) helix (φ = −75°, ψ = 150°). The difference between those two secondary structures resides in the amide bond planar chirality (as illustrated in Table 5).

The values of ϕ, ψ, and ω dihedral angles and the C$\alpha_{(i)}$–C$\alpha_{(i+3)}$ distances in CPM$_1$ have been reported in Table 5. In principle, the use of *N*-(*R*)-(1-phenylethyl) side chains would form CPM'$_1$ loops (present in the hypothetical *ent*-[**28a**·Na]$^+$).

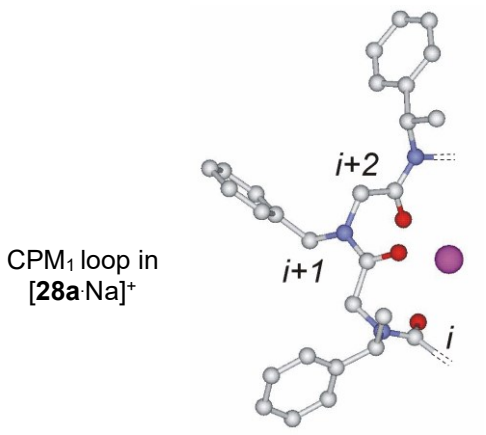

Figure 21. CPM_1 loop present in the minimum energy structures of [**28a**·Na]$^+$. Hydrogen atoms are omitted for clarity. Atom type: C light grey, N blue, O red, Na magenta.

Table 5. Central residues dihedral angles values, amide bonds planar chirality and $C\alpha_{(i)}$–$C\alpha_{(i+3)}$ distances for the CPM_1 and CPM'_1 loops in [**28a**·Na]$^+$/[**30a**·Na]$^+$ and PPII helix

Compound	Loop type	ω_{i+1} (planar chirality)	ϕ_{i+1}	ψ_{i+1}	ω_{i+2} (planar chirality)	ϕ_{i+1}	ψ_{i+1}	Distance $C\alpha_{(i)}$-$C\alpha_{(i+3)}$ in Å
[**28**·Na]$^+$	CPM_1	174.2 ($_pR$)	–71.5	175.0	–173.5 ($_pS$)	70.5	–174.5	7.59
[**30**·Na]$^+$	CPM_1	176.7 ($_pR$)	–73.1	175.4	–179.2 ($_pS$)	75.4	–176.1	7.59
-	CPM_1[a]	180 ($_pR$)	–70	175	180 ($_pS$)	70	–175	>7.0
-	left handed PPII helix	180 ($_pS$)	–75	150	-	-	-	-
[*ent*-**28**·Na]$^+$ / [*ent*-**30**·Na]$^+$	CPM'_1[a]	180 ($_pS$)	70	–175	180 ($_pR$)	–70	175	>7.0

[a] idealized torsion angles values

Sodium Complexation Studies on Octameric Cyclic Peptoid Models. Conformationally stable all-*trans* metallated species were formed by addition of two equivalents of sodium ions to **35** and **36**,[3c,22,28] as suggested by the methine proton chemical shift values of ($\delta < 5.0$) and the relatively small $\Delta\delta$ recorded for the diastereotopic benzyl protons ($\Delta\delta < 0.16$, Figure 22 and titration experiments in Figures S5 and S6).

Addition of a single equivalent of NaTFPB gave a complex mixture of multiple species in slow equilibrium on the NMR time scale.

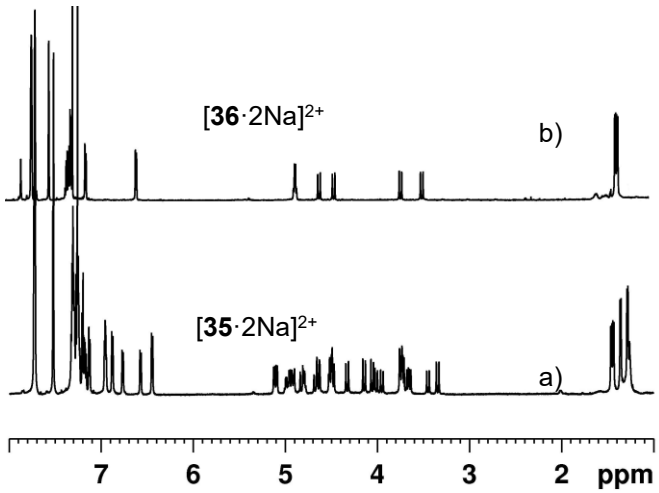

Figure 22. ^{1}H NMR spectra of a) [**35**·2Na]$^{2+}$ and b) [**36**·2Na]$^{2+}$ complexes as NaTFPB^{-} salts in $CDCl_3$ (600 MHz, 8.0–1.0 ppm expansion).

The presence of two metallated species in the ^{1}H NMR spectrum of **35** (Figure 22a) attested the formation of two nonequivalent almost isoenergetic conformational isomers [**35a**·2Na]$^{2+}$ and [**35b**·2Na]$^{2+}$ in a 58:42 ratio (Figure 23). For symmetry reason, only *one* C_4-symmetric *all*-trans species can be formed for the homooligomeric [**36a**·2Na]$^{2+}$ complex (simultaneous inversion of all the amide bonds does not change the structure, Figure 23, log K_{ass} = 6.3, $\Delta G°$ = –8.6 kcal mol^{-1}, calculated by ^{1}H NMR, 3.0 mM host/6.0 mM guest solutions in $CDCl_3$, see SI).

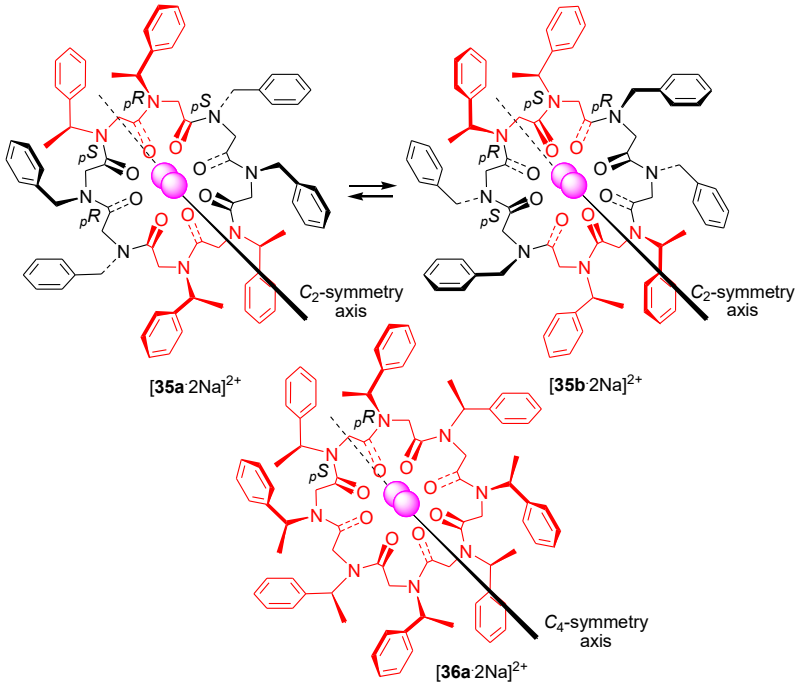

Figure 23. Schematic structures of [**35a**·2Na]$^{2+}$, [**35b**·2Na]$^{2+}$ and [**36a**·2Na]$^{2+}$ with chiral residues in red (Na^+ ions as the magenta sphere).

For the large cavity present in octamer cyclopeptoids, the structures of the complexes can be described as the average of multiple fluxional conformations in fast equilibrium on NMR time scale (as in the case of the non-symmetric minimum energy structures calculated for the *cyclo*-(*N*be$_8$) sodium complexes).[22] The dynamic of this process cannot be described by the static structures of theoretical studies.

Another significant consequence of the fast dynamic equilibria of the sodium cation(s) inside the cavity of cyclic octamer peptoids is the intrinsic difficulty to form single crystals of the metal complexes suitable for X-ray diffractometric studies.[3c,22] After multiple failed attempts to obtain crystals from solutions of **36** as mono- or disodium complexes, we decided to use the smaller PF_6^- as the sodium counterion (used in the past by our group to facilitate the crystallization of prolinated cyclic peptoids).[29] Quantitative addition of a *single* equivalent of $NaPF_6$ to the host **36** (in $CDCl_3$:CD_3CN (9:1), Figure 24 and Figure S7) showed the formation of an unexpected four-fold symmetric species, in slow equilibrium with the free host on the NMR

time scale (log K_{ass} = 4.5, $\Delta G°$ = –6.2 kcal mol^{-1}, calculated by ^{1}H NMR, 3.0 mM host/3.0 mM guest solutions).

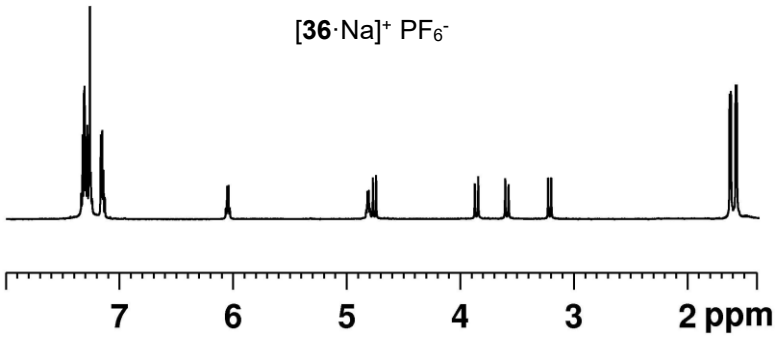

Figure 24. ^{1}H NMR spectra showing cyclic peptoid [**36**·Na]$^+$ PF_6^- in CD_3CN:$CDCl_3$ (9:1) (600 MHz, 8.0–1.0 ppm expansion).

The presence of *cis* and *trans* amide junctions (in a 1:1 ratio) was deduced by the side chain methine proton chemical shift values (δ 5.94, for the *cis* amide bond, and 4.76, for the *trans* amide bond). The two only possible four-fold symmetric conformational isomers compatible with the spectral data were the C_4-symmetric *ctctctct*-[**36b**·Na]$^+$ PF_6^- and *ctctctct*-[**36c**·Na]$^+$ PF_6^- complexes (Figure 25) reminiscent of the rare peptoid ribbon-like structure,[7a] the "η-helix"[30], or the mixed *cis-trans* α,β-oligopeptoids[31] secondary structures.

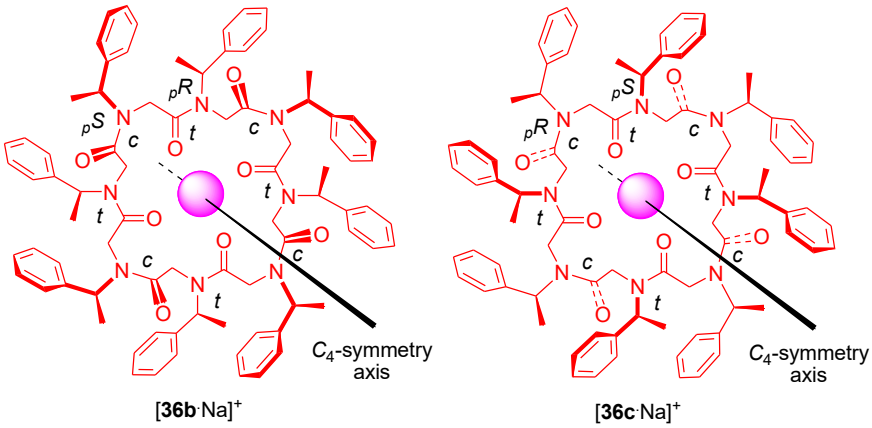

Figure 25. Schematic structures of [**36b**·Na]$^+$ PF_6^- and [**36c**·Na]$^+$ PF_6^- conformational isomers (Na^+ ion is the magenta sphere).

Dissolution of **36** in hot acetonitrile and addition of one equivalent of $NaPF_6$ afforded single crystals suitable for X-ray analysis. Relevant crystallographic data and structure refinement details are listed in

Table S4 (SI). Single crystal X-rays diffraction analysis revealed the formation of a 1:1 Na^+ cyclopeptoid complex with the unprecedented *ctctctct* peptoid bond sequence detected by ^1H NMR spectroscopy and structurally similar to complex [**36b**·Na]$^+$ PF_6^-.

The tetragonal crystalline unit cell contains two symmetry independent [**36b**·Na(H_2O)]$^+$ PF_6^- moieties (Figure 26). Na^+ ions are located on the crystallographic fourfold rotation axes and are hexacoordinated to four *trans* carbonyl oxygen atoms of the macrocycle, to one water molecule and one PF_6^- fluorine atom. Interestingly the side chain groups are alternately directed on opposite faces of the macrocycle providing a pocket where PF_6^- ion is located. Moreover, [**36b**·Na(H_2O)]$^+$ PF_6^- moieties are aligned along the *c* axis by means of CH···OC hydrogen bonds between *cis* carbonyl groups and aromatic *p*-hydrogen atoms, forming channels parallel to the *c* axis, where acetonitrile molecules are located.

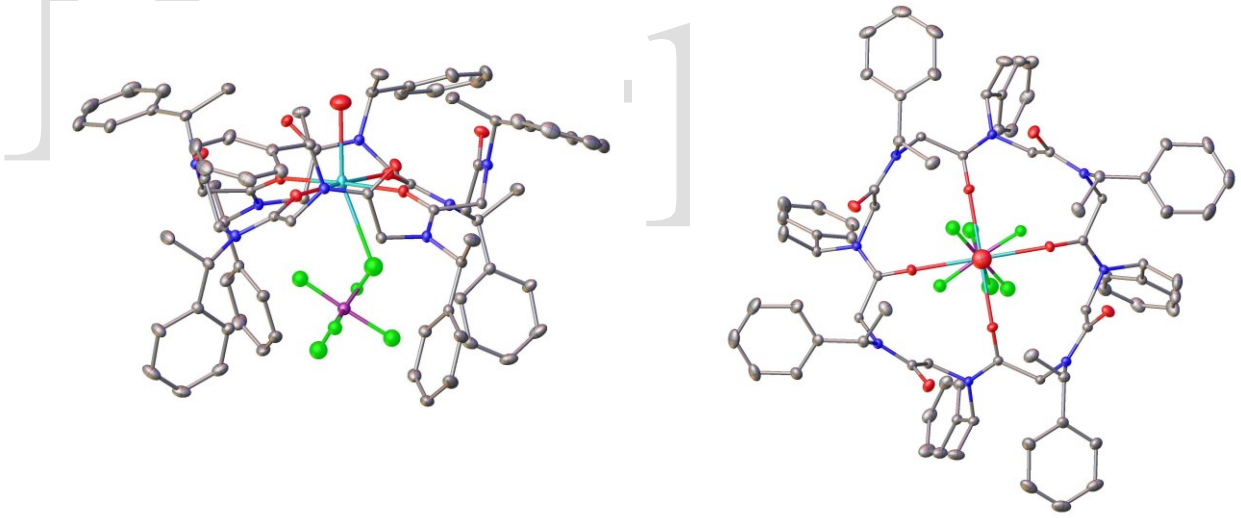

a) b)

Figure 26. ORTEP drawing of [**36b**·Na(H_2O)]$^+$ PF_6^-: a) side view; b) top view. Ellipsoids are drawn at 10% probability level. For clarity hydrogen atoms have been omitted and only one possible disordered PF_6^- moiety is displayed. Atom type: C grey, N blue, O red, P magenta, F green.

The loop structure evident in the X-ray structure (CPM_2 loop) is exemplified in Figure 27. Table 6 reports the values of the ϕ, ψ, and ω dihedral angles of the solid state complex [**36b**·Na(H_2O)]$^+$ PF_6^-. The use of *N*-

(*R*)-(1-phenylethyl) side chains would have formed the hypothetical *ent*-[**36b**·Na(H$_2$O)]$^+$ PF$_6^-$, with an enantiomorphous CPM'$_2$ loop.

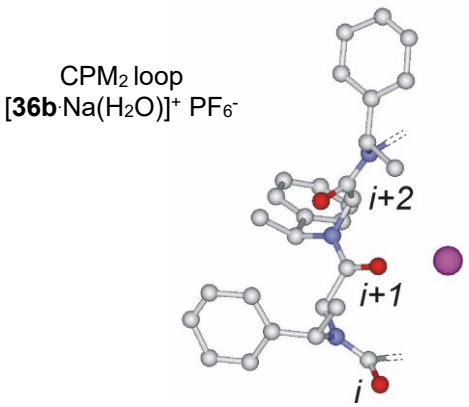

Figure 27. Model of the CPM$_2$ loop present in the solid state structure of [**36b**·Na(H$_2$O)]$^+$ PF$_6^-$. Hydrogen atoms are omitted for clarity. Atom type: C light grey, N blue, O red, Na magenta.

Table 6. Central residues dihedral angles values, amide bonds planar chirality and Cα$_{(i)}$−Cα$_{(i+3)}$ distance for the CPM$_2$ and CPM'$_2$ loops

Compound	Loop type	ω_{i+1} (planar chirality)	ϕ_{i+1}	ψ_{i+1}	ω_{i+2} (planar chirality)	ϕ_{i+1}	ψ_{i+1}	Distance Cα$_{(i)}$-Cα$_{(i+3)}$ in Å
[**36b**·Na(H$_2$O)]$^+$	CPM$_2$	−4.6 ($_p$*S*)	−81.5	−164.1	172.5 ($_p$*R*)	−67.7	170.4	7.94
-	CPM$_2$[a]	0 ($_p$*S*)	−80	−165	180 ($_p$*R*)	−70	170	>7.0
ent[**36b**·Na(H$_2$O)]$^+$	CPM'$_2$[a]	0 ($_p$*R*)	80	165	180 ($_p$*S*)	70	−170	>7.0

[a] idealized values

The unique bond arrangement of the *ctctctct*-[**36b**·Na(H$_2$O)]$^+$ PF$_6^-$ complex recapitulates the major structural traits of cyclic peptoid foldamers. In this species, *S* side chains pair with (*cis*,$_p$*S*)- and (*trans*,$_p$*R*)-amide bonds, metal-dipole electrostatic bonds and Ph(Me)NC−H···O=C hydrogen bonds stabilize the oligoamide scaffold, and torsion angles $\chi_1 \approx -130°$ optimize the side chain/backbone geometry. Structural data also confirm that *cis*- and *trans*-amide bonds induce similar ϕ and ψ torsion angles values.[12e]

The combined sets of conformational preferences emerging in complex [**36b**·Na]$^+$ proves that understanding the relationships between sequence and topological order in peptoid foldamers allows prediction of their secondary structures.

CONCLUSIONS

Since the first synthesis of peptoids, considerable efforts have been devoted to the generation of stable folded oligomers. The biological and pharmacological applications of this class of peptidomimetics are, in fact, strictly dependent on the ability to control their shape and conformational properties. In this contribution we have examined how the concurrent presence of chiral aromatic residues, head-to-tail cyclization, and metal chelation are capable of shaping the topological order of three dimensional oligoamide-based architectures. While stereoelectronic effects in linear peptoid structures induce regular patterns on oligomers with more than 5 or even 8 residues, in cyclic peptoids it is possible to obtain stable folding even in trimeric and tetrameric oligomers. Conformational preferences in larger cyclooligoamides (with six or eight residues) are strictly dependent on the amount and relative position of *N*α-chiral aromatic side chains and vary remarkably in the presence of chelating cations. Weak intramolecular forces emerging from adjacent residues, when exalted by covalent constraints induced by cyclization or by efficient ion-dipole forces, can be used to effectively modulate reverse turn and loop conformations and provide new ways to design non-repetitive architectures complementing the studies made on helix secondary or higher order structures.

Ongoing work in our laboratory is focused on applying these design principles to expand the peptoid three-dimensional chemical space in the frame of the pervading conformational isomerism, the proper conceptual scheme for future application of peptoids in all the fields of science.

EXPERIMENTAL SECTION

Synthesis. *General methods*. Starting materials and reagents purchased from commercial suppliers were generally used without purification unless otherwise mentioned. HPLC analyses were performed on a JASCO LC-NET II/ADC equipped with a JASCO Model PU-2089 Plus Pump and a JASCO MD-2010 Plus UV-vis multiple wavelength detector set at 220 nm. The column used was a C_{18} reversed-phase analytical column (Waters, Bondapak, 10 μm, 125 Å, 3.9 mm × 300 mm) run with linear gradients of ACN (0.1% TFA) into H_2O (0.1% TFA) over 30 min, at a flow rate of 1.0 mL/min for the analytical runs. ESI-MS analysis in positive ion mode was performed using a Finnigan LCQ Deca ion trap mass spectrometer (ThermoFinnigan, San Josè, CA, USA) and the mass spectra were acquired and processed using the Xcalibur software provided by Thermo Finnigan. Samples were dissolved in 1:1 CH_3OH/H_2O, 0.1 % formic acid, and infused in the ESI source by using a syringe pump; the flow rate was 5 μl/min. The capillary voltage was set at 4.0 V, the spray voltage at 5 kV, and the tube lens offset at -40 V. The capillary temperature was 220 °C. Data were acquired in MS1 and MSn scanning modes. Zoom scan was used in these experiments. High-resolution mass spectra (HRMS) were recorded on a Bruker Solarix XR Fourier transform ion cyclotron resonance mass spectrometer (FTICR-MS) equipped with a 7T magnet, using electrospray ionization (ESI). Elemental analyses were performed with a Thermo FlashEA 1112 Series CHNS-O analyzer by Thermo Fisher Scientific Inc. (Waltham, MA, USA); the samples were analyzed after extensive drying in vacuo. Yields refer to chromatographically and spectroscopically (^{1}H- and ^{13}C NMR) pure materials. NMR spectra were recorded on a Bruker DRX 600 (^{1}H at 600.13 MHz, ^{13}C at 150.90 MHz), Bruker DRX 400 (^{1}H at 400.13 MHz, ^{13}C at 100.03 MHz). Chemical shifts (δ) are reported in ppm relative to the residual solvent peak ($CHCl_3$, δ = 7.26; $^{13}CDCl_3$, δ = 77.00; C_2DHCl_4, TCDE, δ = 5.80; CD_3SOCD_2H, DMSO, δ = 2.50; $(^{13}CD_3)_2SO$, DMSO, δ = 39.51, CD_2HCN, δ = 1.94 ppm; $C_6D_5CD_2H$, toluene, δ = 2.09; $C_6D_5{}^{13}CD_3$, toluene, δ = 20.4) and the multiplicity of each signal is designated by the

following abbreviations: s, singlet; d, doublet; dd, double doublet; t, triplet; sept, septet; m, multiplet; br, broad. 2D NMR experiments such as COSY, ROESY, HSQC and HMBC were performed for the full assignment of each signal. Coupling constants (*J*) are quoted in Hertz.

General procedure for the solid-phase synthesis of linear peptoids ***3, 6, 7, 18, 21, 22, 24, 25, 26, 31, 32, 33***. The 2-chlorotrityl chloride resin (α-dichlorobenzhydryl-polystyrene cross-linked with 1% DVB; 100–200 mesh; 1.63 mmol g^{-1}, 0.300 g, 0.489 mmol) was swelled in dry CH_2Cl_2 (3 mL) for 45 min and washed twice with dry CH_2Cl_2 (3 mL). The first submonomer was attached onto the resin by adding bromoacetic acid (0.109 g, 0.782 mmol) in dry CH_2Cl_2 (3 mL) and DIPEA (426 μL, 2.44 mmol) on a shaker platform for 60 min at room temperature, followed by washing with DMF (3 × 1 min), CH_2Cl_2 (3 × 1 min) and then again with DMF (3 × 1 min). A solution of the chosen amine (1.6 M in dry DMF, 3 mL) was added to the bromoacetylated resin. The mixture was left on a shaker platform for 40 min at room temperature, then the resin was washed with DMF (3 × 1 min), CH_2Cl_2 (3 × 1 min) and then again with DMF (3 × 1 min). Subsequent bromoacetylation reactions were accomplished by reacting the aminated oligomer with a solution of bromoacetic acid (0.679 g, 4.89 mmol) and DIC (0.83 mL, 5.38 mmol) in dry DMF (3 mL) for 60 min at room temperature. The filtrated resin was washed with DMF (4 × 1 min), CH_2Cl_2 (4 × 1 min), DMF (4 × 1 min) and treated again with the proper amine under the same conditions reported above. This cycle of reactions was iterated until the target linear oligomer was obtained. The cleavage was performed treating the resin, previously washed with CH_2Cl_2 (3 × 1 min), three times with a solution of HFIP in CH_2Cl_2 (20% v/v, 3.0 mL each time) on a shaker platform at room temperature for 30 min each time. The resin was then filtered away and the combined filtrates were concentrated in vacuo. 1 mg of the final products were dissolved in 60 μL of acetonitrile (0.1% TFA) and 60 μL of HPLC grade water (0.1% TFA) and analyzed by RP-HPLC; purity >80% (except for **31**, 46%); conditions: 5 → 100% A in 30 min for the all oligomers (A, 0.1% TFA in acetonitrile, B, 0.1% TFA in water); flow: 1.0 mL min^{-1}, 220 nm]. The linear oligomers (isolated as

amorphous solids) were subjected to ESI mass spectrometry and, subsequently, to the cyclization reactions without further purification.

H-*N*pm-*N*spe-*N*pm-OH (**3**): white amorphous solid, 0.231 g, 100% yield; t_R: 7.1 min. ES-MS *m/z*; 474.2 $[M + H]^+$, HRMS (ESI/FTICR) *m/z*; $[M + H]^+$ Calcd for $C_{28}H_{32}N_3O_4^+$ 474.2387; Found 474.2375.

H-*N*pm-*N*spe$_2$-OH (**6**): white amorphous solid, 0.238 g, 100% yield; t_R: 8.1 min. ES-MS *m/z*; 448.2 $[M + H]^+$, HRMS (ESI/FTICR) *m/z*; $[M + H]^+$ Calcd for $C_{29}H_{34}N_3O_4^+$ 488.2544; Found 488.2538.

H-*N*spe$_3$-OH (**7**): white amorphous solid, 0.245 g, 100% yield; t_R: 8.0 min. ES-MS *m/z*; 502.6 $[M + H]^+$, HRMS (ESI/FTICR) *m/z*; $[M + H]^+$ Calcd for $C_{30}H_{36}N_3O_4^+$ 502.2700; Found 502.2709.

H-*N*pm$_2$-*N*spe-*N*pm-OH (**18**): white amorphous solid, 0.303 g, 100% yield; t_R: 8.7 min. ES-MS *m/z*; 621.0 $[M + H]^+$, HRMS (ESI/FTICR) *m/z*; $[M + H]^+$ Calcd for $C_{37}H_{41}N_4O_5^+$ 621.3071; Found 621.3079.

H-*N*spe-*N*pm-*N*spe-*N*pm-OH (**21**): white amorphous solid, 0.310 g, 100% yield; t_R: 8.7 min. ES-MS *m/z*; 635.3 $[M + H]^+$, HRMS (ESI/FTICR) *m/z*; $[M + H]^+$ Calcd for $C_{38}H_{43}N_4O_5^+$ 635.3228; Found 635.3219.

H-*N*spe$_4$-OH (**22**): white amorphous solid, 0.324 g, 100% yield; t_R: 9.4 min. ES-MS *m/z*; 662.9 $[M + H]^+$, HRMS (ESI/FTICR) *m/z*; $[M + H]^+$ Calcd for $C_{40}H_{47}N_4O_5^+$ 663.3541; Found 663.3553.

H-*N*pm$_4$-*N*spe-*N*pm-OH (**24**): white amorphous solid, 0.268 g, 60% yield; t_R: 11.5 min. ES-MS *m/z*; 915.4 $[M + H]^+$, HRMS (ESI/FTICR) *m/z*; $[M + H]^+$ Calcd for $C_{55}H_{59}N_6O_7^+$ 915.4440; Found 915.4460.

H-(*N*spe-*N*pm)$_3$-OH (**25**): white amorphous solid, 0.461 g, 100% yield; t_R: 11.8 min. ES-MS *m/z*; 943.5 $[M + H]^+$, HRMS (ESI/FTICR) *m/z*; $[M + H]^+$ Calcd for $C_{57}H_{63}N_6O_7^+$ 943.4753; Found 943.4730.

H-*N*spe$_6$-OH (**26**): white amorphous solid, 0.481 g, 100% yield; t_R: 12.8 min. ES-MS *m/z*; 985.5 $[M + H]^+$, HRMS (ESI/FTICR) *m/z*; $[M + H]^+$ Calcd for $C_{60}H_{69}N_6O_7^+$ 985.5222; Found 985.5201.

H-*N*pm$_6$-*N*spe-*N*pm-OH (**31**): white amorphous solid, 0.532 g, 90% yield; t_R: 13.3 min. ES-MS

m/z; 1210.5 $[M + H]^+$, HRMS (ESI/FTICR) *m/z*; $[M + H]^+$ Calcd for $C_{73}H_{77}N_8O_9^+$ 1209.5808; Found 1209.5839.

H-*N*pm-*N*spe$_2$-*N*pm$_2$-*N*spe$_2$-*N*pm-OH (**32**): white amorphous solid, 0.483 g, 79% yield; t_R: 13.1 min. ES-MS *m/z*; 1252.7 $[M + H]^+$, HRMS (ESI/FTICR) *m/z*; $[M + H]^+$ Calcd for $C_{76}H_{83}N_8O_9^+$ 1251.6278; Found 1251.6299.

H-*N*spe$_8$-OH (**33**): white amorphous solid, 0.639 g, 100% yield; t_R: 14.1 min. ES-MS *m/z*; 1307.7 $[M + H]^+$, HRMS (ESI/FTICR) *m/z*; $[M + H]^+$ Calcd for $C_{80}H_{91}N_8O_9^+$ 1307.6904; Found 1307.6943.

General procedure for the high dilution cyclization of ***1/2, 8, 9, 16/17, 19, 27, 28, 30, 34, 35, 36***. Solutions of linear peptoids (0.150 mmol), previously co-evaporated three times with toluene, were prepared under nitrogen in dry DMF (5.0 mL). The mixture was added dropwise to a stirred solution of HATU (0.228 g, 0.600 mmol) and DIPEA (162 µL, 0.930 mmol) in dry DMF (45.0 mL) by a syringe pump in 3 h, at room temperature in anhydrous atmosphere. After 12 h the resulting mixture was concentrated *in vacuo*, diluted with CH_2Cl_2 (30 mL), washed twice with a solution of HCl (1.0 M, 15 mL). The organic phase was washed with water (30.0 mL), dried over anhydrous $MgSO_4$, filtered and concentrated *in vacuo*. The crude peptoids were analysed *via* ^{1}H NMR. The crude cyclic peptoids **16/17**, **19**, **27**, **28**, **30**, **34** were dissolved in hot acetonitrile and precipitated by slowly cooling the acetonitrile solutions. Crude **35**, **36** were purified on reverse silica gel (C_{18}); conditions: 10% – 100% A (A: acetonitrile; B: water). Crude **1/2**, **8**, **9** were purified on flash silica gel; conditions: 10% – 50% A (A: ethyl acetate; B: petroleum ether). Cyclic peptoids were dissolved in 50% acetonitrile in HPLC grade water and analyzed by RP-HPLC; purity >90% conditions: 5% – 100% A in 30 min (A, 0.1% TFA in acetonitrile, B, 0.1% TFA in water); flow: 1 mL min^{-1}, 220 nm.

Note: **16/17**, **19**, **27**, **28** chromatograms are not reported due to the insolubility of the compounds in the acetonitrile solutions. Their analytical purity was corroborated by the elemental analysis.

Further cyclization procedures for ***6, 7, 22***.[28b,32] a) PyBOP/DIPEA. Solutions of linear peptoids (0.150 mmol), previously co-evaporated three times with toluene, were prepared under nitrogen in dry DMF (5.0 mL). The mixture was added dropwise to a stirred solution of PyBOP (0.242 g, 0.465 mmol) and DIPEA (162 μL, 0.930 mmol) in dry DMF (70.0 mL) by a syringe pump in 3 h, at room temperature in anhydrous atmosphere. After 12 h the resulting mixture was concentrated *in vacuo*, diluted with CH_2Cl_2 (30 mL), washed twice with a solution of HCl (1.0 M, 15 mL). The organic phase was washed with water (30.0 mL), dried over anhydrous $MgSO_4$, filtered and concentrated *in vacuo*. b) EDC/HOBt/TEA. Solutions of linear peptoids (0.150 mmol), previously co-evaporated three times with toluene, were prepared under nitrogen in dry DMF (5.0 mL). The mixture was added dropwise to a stirred solution of EDC (0.172 g, 0.900 mmol), HOBt (0.122 g, 0.900 mmol) and dry triethylamine (125 μL, 0.900 mmol) in dry DMF (45.0 mL) by a syringe pump in 3 h, at room temperature in anhydrous atmosphere. After 12 h the resulting mixture was concentrated *in vacuo*, diluted with CH_2Cl_2 (30 mL), washed twice with a solution of HCl (1.0 M, 15 mL). The organic phase was washed with water (30.0 mL), dried over anhydrous $MgSO_4$, filtered and concentrated *in vacuo*. The crude material from the cyclization procedures contained a complex mixture of unidentified compounds.

Cyclo-[(*cis*,$_p$*S*)*N*spe-(*cis*,$_p$*S*)*N*pm-(*cis*,$_p$*S*)*N*pm)] (**1**) and *cyclo*-[(*cis*,$_p$*R*)*N*spe-(*cis*,$_p$*R*)*N*pm-(*cis*,$_p$*R*)*N*pm)] (**2**): white amorphous solid, 0.013 g, 19% yield; t_R: 8.9 min. ^{1}H NMR (600 MHz, $(CD_3)_2SO$, as a 70/30 mixture of „crown“ conformational isomers) δ: 7.35-7.22 (15H, br signals, Ar-*H*), 5.47 (0.7H, q, *J* 6.9 Hz, N-C*H*CH_3-Ph), 5.32 (0.3H, d, *J* 15.9 Hz, N-CH_2-Ph or O=C-CH_2-N), 5.21 (1.3H, overlapping, N-CH_2-Ph and/or O=C-CH_2-N), 5.16 (1.3H, br d, N-CH_2-Ph and/or O=C-CH_2-N), 5.10 (1H, overlapping, N-CH_2-Ph and/or O=C-CH_2-N plus N-C*H*CH_3-Ph of the minor isomer), 5.03 (1.3H, overlapping, N-CH_2-Ph and/or O=C-CH_2-N), 4.23 (0.7H, d, *J* 14.8 Hz, N-CH_2-Ph and/or O=C-CH_2-N), 4.19 (0.3H, d, *J* 15.0 Hz, N-CH_2-Ph and/or O=C-CH_2-N), 4.14 (0.3H, d, *J* 15.2 Hz, N-CH_2-Ph and/or O=C-CH_2-N), 4.10 (0.7H, d, *J* 14.8 Hz, N-CH_2-Ph and/or O=C-CH_2-N), 3.82 (0.7H, overlapping, N-CH_2-Ph and/or O=C-CH_2-N) 3.46-

3.38 (2.4H, overlapping, N-C*H*$_2$-Ph and/or O=C-C*H*$_2$-N), 1.63 (0.9H, d, *J* 7.1 Hz, N-CHC*H*$_3$-Ph), 1.56 (2.1H, d, *J* 7.0 Hz, N-CHC*H*$_3$-Ph); ^{13}C{^{1}H} NMR (150 MHz, $(CD_3)_2SO$, as a 70/30 mixture of „crown" conformational isomers) δ: 169.5, 168.5, 168.2, 140.6, 137.0 (x2), 128.9 (multiple signals), 128.7 (multiple signals), 128.4 (multiple signals), 128.3 (multiple signals), 127.9, 127.7, 126.9, 126.8, 79.6, 58.1, 55.0, 51.4, 50.0, 49.7, 49.5, 49.4, 48.7, 48.4, 48.2, 47.2, 17.6, 16.4. HRMS (ESI/FTICR) *m/z*; $[M + H]^+$ Calcd for $C_{28}H_{30}N_3O_3^+$ 456.2282; Found 456.2290.

4-Benzyl-3,4,5,6-tetrahydro-1,5-bis((S)-1-phenylethyl)-1H-pyrrolo[2,3-b]pyrazine-2,7-dione (**8**): white amorphous solid, 0.017 g, 25% yield; t_R: 11.2 min. ^{1}H NMR (600 MHz, $CDCl_3$) δ: 7.42-7.18 (15H, overlapping, Ar-*H*), 6.24 (1H, q, *J* 7.1 Hz, C=O-N-C*H*CH$_3$-Ph), 4.92 (1H, q, *J* 7.1 Hz, C=O-N-C*H*CH$_3$-Ph), 4.65 (1H, d, *J* 15.4 Hz, N-C*H*H-Ph), 4.55 (1H, d, *J* 15.4 Hz, N-CH*H*-Ph), 3.89 (1H, d, *J* 16.3 Hz, C=O-C*H*H-N-Bn), 3.76 (1H, d, *J* 16.3 Hz, C=O-CH*H*-N-Bn), 3.61 (1H, d, *J* 18.1 Hz, C=O-C*H*H-N-CHCH$_3$-Ph), 3.46 (1H, d, *J* 18.1 Hz, C=O-CH*H*-N-CHCH$_3$-Ph), 1.82 (3H, d, *J* 7.1 Hz, C=O-N-CHC*H*$_3$-Ph), 1.55 (3H, d, *J* 7.1 Hz, C=O-N-CHC*H*$_3$-Ph); ^{13}C{^{1}H} NMR (150 MHz, $CDCl_3$) δ: 180.6, 165.7, 160.2, 141.7, 139.3, 135.1, 129.7 (x2), 129.3 (x2), 129.0, 128.6, 128.2 (x2), 127.9 (x2), 127.5 (x2), 127.1, 126.9 (x2), 105.7, 56.3 (x2), 54.6, 53.5, 52.4, 17.0 (x2). HRMS (ESI/FTICR) *m/z*; $[M + H]^+$ Calcd for $C_{29}H_{30}N_3O_2^+$ 452.2333; Found 452.2320.

3,4,5,6-tetrahydro-1,4,5-tris((S)-1-phenylethyl)-1H-pyrrolo[3,2-b]pyrazine-2,7-dione (**9**): white amorphous solid, 0.018 g, 26% yield; t_R: 10.1 min. ^{1}H NMR (600 MHz, $CDCl_3$) δ: 7.43-7.18 (15H, overlapping, Ar-*H*), 6.07 (1H, q, *J* 7.2 Hz, N-C*H*CH$_3$-Ph), 5.07 (1H, q, *J* 7.2 Hz, N-C*H*CH$_3$-Ph), 4.97 (1H, q, *J* 7.2 Hz, N-C*H*CH$_3$-Ph), 3.76 (1H, d, *J* 16.2 Hz, C-3*H*H), 3.68 (2H, br d, overlapping, C-3H*H* and C-6*H*H), 3.46 (1H, d, *J* 18.2 Hz, C-6H*H*), 1.69 (3H, d, *J* 7.2 Hz, C=O-N-CHC*H*$_3$-Ph), 1.66 (3H, d, *J* 7.2 Hz, C=O-N-CHC*H*$_3$-Ph), 1.64 (3H, d, *J* 7.2 Hz, C=O-N-CHC*H*$_3$-Ph); ^{13}C{^{1}H} NMR (150 MHz, $CDCl_3$) δ: 181.5, 166.1, 160.1, 141.1, 139.1, 138.4, 129.1 (x2), 129.0 (x2), 128.5, 128.3, 127.7 (x2), 127.5 (x2), 126.6

(x3), 126.4 (x2), 106.7, 58.8, 56.0, 53.8, 51.7, 48.0, 17.4, 16.8, 16.3. HRMS (ESI/FTICR) *m/z*; $[M + H]^+$ Calcd for $C_{30}H_{32}N_3O_2^+$ 466.2489; Found 466.2475.

(*S*)-3,4,5,6-tetrahydro-3-hydroxy-1,4,5-tris((*S*)-1-phenylethyl)-1H-pyrrolo[2,3-b]pyrazine-2,7-dione (**15**): white crystalline solid. ^{1}H NMR (600 MHz, $CDCl_3$) δ: 7.39-7.15 (15H, overlapping, Ar-*H*), 6.16 (1H, q, *J* 7.0 Hz, N-1-C*H*CH_3-Ph), 5.21 (1H, q, *J* 7.2 Hz, N-4-C*H*CH_3-Ph), 5.09 (1H, s, CHO*H*), 5.03 (1H, q, *J* 7.2 Hz, N-5-C*H*CH_3-Ph), 3.62 (1H, d, *J* 18.0 Hz, C*H*H), 3.31 (1H, d, *J* 18.0 Hz, CH*H*), 1.92 (3H, d, *J* 7.2 Hz, N-4-CHC*H*$_3$-Ph), 1.72 (3H, d, *J* 7.2 Hz, N-5-CHC*H*$_3$-Ph), 1.68 (3H, d, *J* 7.0 Hz, N-1-CHC*H*$_3$-Ph); ^{13}C{^{1}H} NMR (150 MHz, $CDCl_3$) δ: 181.5, 163.4, 160.0, 140.5, 139.9, 137.6, 129.2 (x3), 128.9 (x3), 127.7 (x3), 127.3 (x2), 127.1 (x2), 126.2 (x2), 104.4, 78.6, 57.8, 56.6, 53.4, 51.4, 17.9, 17.6, 15.9. HRMS (ESI/FTICR) *m/z*; $[M + H]^+$ Calcd for $C_{30}H_{32}N_3O_3^+$ 482.2438; Found 482.2429.

Cyclo-[(*cis*,$_p$*R*)*N*pm-(*trans*,$_p$*R*)*N*pm-(*cis*,$_p$*S*)*N*spe-(*trans*,$_p$*S*)*N*pm] (**16**) and *cyclo*-[(*cis*,$_p$*S*)*N*pm-(*trans*,$_p$*S*)*N*pm-(*cis*,$_p$*R*)*N*spe-(*trans*,$_p$*R*)*N*pm] **(17)**: white amorphous solid, 0.037 g, 41% yield. ^{1}H NMR (600 MHz, $CDCl_3$, conformational isomers ratio: 85/15; note: the only reported ^{1}H NMR signals of the minor conformational isomer are those of the C<u>H</u>C<u>H</u>$_3$ resonances, the other resonances are hidden under the peaks of the major conformational isomer) δ: 7.34-7.20 (12H, br signals, Ar-*H*), 7.11-7.03 (8H, br signals, Ar-*H*), 5.92 (1H, q, *J* 7.0 Hz, N$_c$-C*H*CH_3-Ph), 5.55 (1H, d, *J* 14.5 Hz, N$_c$-C*H*H-Ph), 5.43 (1H, d, *J* 14.7 Hz, O=C-C*H*H-N$_t$-CH_2-Ph), 5.35 (0.15H, q, *J* 7.0 Hz, N$_c$-C*H*CH_3-Ph, minor conformational isomer), 5.33 (1H, d, *J* 14.6 Hz, O=C-C*H*H-N$_t$-CH_2-Ph), 4.47 (1H, d, *J* 17.2 Hz, N$_t$-C*H*H-Ph), 4.41 (1H, d, *J* 17.8 Hz, O=C-C*H*H-N$_c$-CH_2-Ph), 4.39 (2H, br d, overlapping, N$_t$-C*H*H-Ph and O=C-CH*H*-N$_t$-CH_2-Ph), 4.31 (1H, d, *J* 17.2 Hz, N$_t$-CH*H*-Ph), 4.22 (1H, d, *J* 18.4 Hz, O=C-C*H*H-N$_c$-$CHCH_3$-Ph), 3.77 (1H, d, *J* 14.5 Hz, N$_c$-CH*H*-Ph), 3.51 (1H, d, *J* 14.7 Hz, O=C-CH*H*-N$_t$-CH_2-Ph), 3.49 (2H, overlapping, O=C-CH*H*-N$_c$-CH_2-Ph and N$_t$-CH*H*-Ph), 3.39 (1H, d, *J* 18.4 Hz, O=C-CH*H*-N$_c$-$CHCH_3$-Ph), 1.47 (0.45H, d, *J* 7.0 Hz, N-CHC*H*$_3$-Ph, minor conformational isomer), 1.45 (3H, d, *J* 7.0 Hz, N$_c$-CHC*H*$_3$-Ph); ^{13}C{^{1}H} NMR (150 MHz, $CDCl_3$; note: only the ^{13}C NMR signals of the major

conformational isomer are reported) δ: 169.4, 169.2, 168.5, 167.9, 140.0, 136.0, 135.8, 135.3, 129.1 (x2), 129.0 (x4), 128.7 (x2), 128.6 (x2), 128.0, 127.9, 127.8 (x2), 127.5 (x2), 126.8 (x2), 126.4 (x2), 52.6, 50.5, 49.6, 49.5 (x3), 47.2, 45.8, 16.6. Anal. Calcd for $C_{37}H_{38}N_4O_4$: C, 73.73; H, 6.35; N, 9.30; Found C, 73.98; H, 6.33; N, 9.28. HRMS (ESI/FTICR) *m/z*; $[M + H]^+$ Calcd for $C_{37}H_{39}N_4O_4^+$ 603.2966; Found 603.2958.

Cyclo-[(*cis*,$_p$*R*)*N*spe-(*trans*,$_p$*R*)*N*pm-(*cis*,$_p$*S*)*N*spe-(*trans*,$_p$*S*)*N*pm] **(19)**: white amorphous solid, 0.017 g, 18% yield. ^{1}H NMR (600 MHz, $CDCl_3$) δ: 7.35-7.18 (15H, br signals, Ar-*H*), 7.01-7.00 (3H, m, Ar-*H*), 6.94 (2H, d, *J* 7.0 Hz, Ar-*H*), 5.86 (1H, q, *J* 7.0 Hz, N_c-C*H*CH_3-Ph), 5.38 (1H, d, *J* 14.2 Hz, O=C-C*H*H-N_t-CH_2-Ph, and 1H, N_c-C*H*CH_3-Ph, overlapping), 5.14 (1H, d, *J* 14.6 Hz, O=C-C*H*H-N_t-CH_2-Ph), 4.50 (1H, d, *J* 17.3 Hz, N_t-C*H*H-Ph), 4.40 (1H, d, *J* 18.1 Hz, O=C-C*H*H-N_c-$CHCH_3$-Ph), 4.38 (1H, d, *J* 17.3 Hz, N_t-C*H*H-Ph), 4.28 (2H, overlapping, d, *J* 17.3 Hz, N_t-CH*H*-Ph and N_t-CH*H*-Ph), 4.20 (1H, d, *J* 18.2 Hz, O=C-C*H*H-N_c-$CHCH_3$-Ph), 3.61 (1H, d, *J* 18.1 Hz, O=C-CH*H*-N_c-$CHCH_3$-Ph), 3.47 (1H, d, *J* 14.2 Hz, O=C-CH*H*-N_t-CH_2-Ph), 3.28 (2H, overlapping, d, *J* 18.2 Hz, O=C-CH*H*-N_t-CH_2-Ph and O=C-CH*H*-N_c-$CHCH_3$-Ph), 1.48 (3H, d, *J* 7.0 Hz, N_c-CHC*H*$_3$-Ph), 1.44 (3H, d, *J* 7.0 Hz, N_c-CHC*H*$_3$-Ph); ^{13}C{^{1}H} NMR (150 MHz, $CDCl_3$) δ: 169.4 (x2), 168.5, 167.2, 140.0, 138.8, 135.7, 135.5, 129.0 (x4), 128.6 (x3), 128.1 (x3), 127.9, 127.4 (x3), 126.6 (x3), 126.4 (x3), 56.3, 52.6, 50.5, 49.7 (x2), 49.4, 46.4, 45.8, 17.1, 16.6. Anal. Calcd for $C_{38}H_{40}N_4O_4$: C, 74.00; H, 6.54; N, 9.08; O, 10.38; Found C, 74.11; H, 6.56; N, 9.06; O, 10.40. HRMS (ESI/FTICR) *m/z*; $[M + H]^+$ Calcd for $C_{38}H_{41}N_4O_4^+$ 617.3122; Found 617.3134.

Cyclo-(*N*spe-*N*pm$_5$) (**27**): white amorphous solid, 0.075 g, 56% yield. ^{1}H NMR (600 MHz, $CDCl_3$, complex mixture of rotamers) δ: 7.39-7.03 (30H, overlapping, Ar-*H*), 5.47-3.24 (23H, overlapping, br signals, N-C*H*CH_3-Ph, O=C-C*H*$_2$-N-$CHCH_3$-Ph, N-C*H*$_2$-Ph, O=C-C*H*$_2$-N-CH_2-Ph), 1.82-1.51 (3H, overlapping, br signals, N-CHC*H*$_3$-Ph); ^{13}C{^{1}H} NMR (150 MHz, $CDCl_3$, complex mixture of rotamers) δ: 171.8, 169.6, 169.5, 169.4, 169.0, 168.9, 168.6, 168.4, 136.8, 136.5, 135.6, 135.4, 135.3, 135.2, 134.9,

129.1, 128.7, 128.4, 127.6, 127.5, 127.3, 125.5, 125.4, 125.2, 53.0, 52.8, 52.7, 51.8, 51.6, 51.4, 51.1, 50.7, 50.4, 50.3, 50.1, 49.7, 49.6, 49.2, 47.7, 46.2, 44.3, 16.3, 15.4. Anal. Calcd for $C_{55}H_{56}N_6O_6$: C, 73.64; H, 6.29; N, 9.37; Found C, 73.47; H, 6.30; N, 9.31. HRMS (ESI/FTICR) *m/z*; $[M + H]^+$ Calcd for $C_{55}H_{57}N_6O_6^+$ 897.4334; Found 897.4350.

Cyclo-[(*cis*,$_p$*R*)*N*pm-(*trans*,$_p$*R*)*N*spe-(*cis*,$_p$*R*)*N*pm-(*cis*,$_p$*S*)*N*spe-(*trans*,$_p$*S*)*N*pm-(*cis*,$_p$*S*)*N*spe] (**28**): white amorphous solid, 0.071 g, 51% yield. ^{1}H NMR (600 MHz, $CDCl_3$, mixture of conformational isomers with 70% of *cctcct*-**28**) δ: 7.42-6.92 (30H, overlapping, Ar-*H*), 5.98 (1H, q, *J* 7.0 Hz, N_c-C*H*CH_3-Ph), 5.74 (1H, q, *J* 6.9 Hz, N_c-C*H*CH_3-Ph), 5.61 (1H, d, *J* 15.0 Hz, N_c-C*H*H-Ph), 5.44 (1H, d, *J* 15.9 Hz, N_c-C*H*H-Ph), 4.90 (1H, d, *J* 18.0 Hz, N_t-C*H*H-Ph), 4.87 (1H, d, *J* 17.8 Hz, O=C-C*H*H-N_c-CH_2-Ph), 4.78 (1H, q, *J* 7.0 Hz, N_t-C*H*CH_3-Ph), 4.72 (1H, d, *J* 15.1 Hz, O=C-C*H*H-N_t-CH_2-Ph), 4.70 (1H, d, *J* 15.0 Hz, O=C-C*H*H-N_t-$CHCH_3$-Ph), 4.55 (1H, d, *J* 18.0 Hz, N_t-CH*H*-Ph), 4.49 (1H, d, *J* 17.9 Hz, O=C-C*H*H-N_c-$CHCH_3$-Ph), 3.96 (1H, d, *J* 15.9 Hz, N_c-CH*H*-Ph), 3.88 (1H, d, *J* 17.8 Hz, O=C-C*H*H-N_c-CH_2-Ph), 3.80 (1H, d, *J* 17.8 Hz, O=C-C*H*H-N_c-$CHCH_3$-Ph), 3.74 (1H, d, *J* 15.0 Hz, N_c-CH*H*-Ph), 3.70 (1H, d, *J* 17.8 Hz, O=C-CH*H*-N_c-CH_2-Ph), 3.68 (1H, d, *J* 17.8 Hz, O=C-CH*H*-N_c-$CHCH_3$-Ph), 3.41 (1H, d, *J* 15.0 Hz, O=C-CH*H*-N_t-$CHCH_3$-Ph), 3.34 (1H, d, *J* 17.8 Hz, O=C-CH*H*-N_c-CH_2-Ph), 3.18 (2H, overlapping, O=C-CH*H*-N_t-CH_2-Ph and O=C-CH*H*-N_c-$CHCH_3$-Ph), 1.81 (3H, d, *J* 7.0 Hz, N_t-CHC*H*$_3$-Ph), 1.43 (3H, d, *J* 6.9 Hz, N_c-CHC*H*$_3$-Ph), 1.41 (3H, d, *J* 7.0 Hz, N_c-CHC*H*$_3$-Ph); ^{13}C{^{1}H} NMR (150 MHz, $CDCl_3$, mixture of conformational isomers with 70% of *cctcct*-**28**) δ: 171.6, 171.5, 170.2, 169.2, 168.2, 168.1, 141.1, 140.8, 138.6, 137.1, 136.8, 135.3, 129.1 (x2), 129.0 (x2), 128.7 (x4), 128.6 (x2), 128.2 (x4), 128.2 (x2), 127.6 (x3), 127.4 (x3), 127.2 (x3), 127.1, 125.4 (x2), 125.0 (x2), 55.4, 54.1, 52.7, 52.0, 51.2 (x2), 50.7, 49.4, 47.8, 45.8, 45.1, 44.8, 20.7, 17.0, 15.8. Anal. Calcd for $C_{57}H_{60}N_6O_6$: C, 74.00; H, 6.54; N, 9.08; O, 10.38; Found C, 74.19; H, 6.57; N, 9.10; O, 10.40. HRMS (ESI/FTICR) *m/z*; $[M + H]^+$ Calcd for $C_{57}H_{61}N_6O_6^+$ 925.4647; Found 925.4670.

Cyclo-[(*cis*,$_p$*R*)*N*spe-(*trans*,$_p$*R*)*N*spe-(*cis*,$_p$*R*)*N*spe-(*cis*,$_p$*S*)*N*spe-(*trans*,$_p$*S*)*N*spe-(*cis*,$_p$*S*)*N*spe] (**30**):

white amorphous solid, 0.048 g, 33% yield; t_R: 15.1 min. ^{1}H-NMR (600 MHz, $CDCl_3$, mixture of conformational isomers with 70% of *cctcct*-**30**) δ: 7.40-7.17 (24H, overlapping, Ar-*H*), 7.05 (2H, d, *J* 7.2 Hz, Ar-*H*), 7.00-6.98 (4H, overlapping, Ar-*H*), 6.05 (1H, q, *J* 7.2 Hz, N_c-C*H*CH_3-Ph), 5.95 (1H, q, *J* 7.2 Hz, N_c-C*H*CH_3-Ph), 5.72 (1H, q, *J* 6.6 Hz, N_c-C*H*CH_3-Ph), 5.30 (1H, q, *J* 6.9 Hz, N_c-C*H*CH_3-Ph), 4.83 (1H, q, *J* 6.9 Hz, N_t-C*H*CH_3-Ph), 4.72 (1H, q, *J* 7.0 Hz, N_t-C*H*CH_3-Ph), 4.54 (1H, d, *J* 17.2 Hz, O=C-C*H*H-N-$CHCH_3$-Ph), 4.51 (1H, d, *J* 16.7 Hz, O=C-C*H*H-N-$CHCH_3$-Ph), 4.49 (1H, d, *J* 15.3 Hz, O=C-C*H*H-N-$CHCH_3$-Ph), 4.27 (1H, d, *J* 15.2 Hz, O=C-C*H*H-N-$CHCH_3$-Ph), 3.55 (1H, d, *J* 18.0 Hz, O=C-C*H*H-N-$CHCH_3$-Ph), 3.52 (1H, d, *J* 15.3 Hz, O=C-CH*H*-N-$CHCH_3$-Ph), 3.50 (2H, br d, overlapping signals, O=C-C*HH*-N-$CHCH_3$-Ph), 3.36 (1H, d, *J* 18.0 Hz, O=C-CH*H*-N-$CHCH_3$-Ph), 3.31 (1H, d, *J* 15.2 Hz, O=C-CH*H*-N-$CHCH_3$-Ph), 3.14 (1H, d, *J* 16.7 Hz, O=C-CH*H*-N-$CHCH_3$-Ph), 3.12 (1H, d, *J* 17.2 Hz, O=C-CH*H*-N-$CHCH_3$-Ph), 1.72 (3H, d, *J* 7.0 Hz, N_t-CHC*H*$_3$-Ph), 1.67 (3H, d, *J* 6.9 Hz, N_t-CHC*H*$_3$-Ph), 1.55 (3H, d, *J* 6.6 Hz, N_c-CHC*H*$_3$-Ph), 1.45 (3H, d, *J* 7.2 Hz, N_c-CHC*H*$_3$-Ph), 1.40 (3H, d, *J* 7.2 Hz, N_c-CHC*H*$_3$-Ph), 1.15 (3H, d, *J* 6.9 Hz, N_c-CHC*H*$_3$-Ph); ^{13}C{^{1}H} NMR (150 MHz, $CDCl_3$, mixture of conformational isomers with 70% of *cctcct*-**30**) δ: 171.5, 171.3, 169.9, 169.0, 168.5, 168.3, 142.0, 141.3, 140.7, 140.5, 139.7, 138.7, 128.9 (x4), 128.7 (x2), 128.5 (x2), 128.1 (x4), 128.0 (x4), 127.6 (x2), 127.4 (x2), 127.2 (x4), 127.1 (x2), 126.6 (x2), 125.4 (x2), 57.9, 55.7, 55.1, 53.8, 51.7, 51.0, 48.9, 47.5, 47.0, 46.8, 46.6, 44.5, 20.4, 20.2, 17.0, 16.6, 16.2, 15.4. HRMS (ESI/FTICR) *m/z*; $[M + H]^+$ Calcd for $C_{60}H_{67}N_6O_6^+$ 967.5117; Found 967.5135.

Cyclo-(*N*spe-*N*pm$_7$) (**34**): white amorphous solid, 0.054 g, 30% yield; t_R: 15.9 min. ^{1}H NMR (400 MHz, $CDCl_3$, complex mixture of rotamers) δ: 7.34-7.22 (32H, overlapping, Ar-*H*), 7.05-7.02 (8H, overlapping, Ar-*H*), 4.63-3.44 (31H, overlapping, N-C*H*CH_3-Ph, N-C*H*$_2$-Ph, O=C-C*H*$_2$-N-CH_2-Ph, O=C-C*H*$_2$-N-$CHCH_3$-Ph), 1.63-1.12 (3H, N-CHC*H*$_3$-Ph); ^{13}C{^{1}H} NMR (150 MHz, $CDCl_3$, complex mixture of rotamers) δ: 170.4, 169.6, 169.4, 168.8, 168.4, 168.0, 167.6, 167.3, 136.6, 136.4, 136.0, 135.7, 129.0, 128.8, 128.6, 127.9, 127.6, 127.4, 126.8, 126.6, 126.4, 126.3, 55.9, 54.8, 53.0, 52.5, 52.2, 51.6, 51.5, 50.4,

50.2, 49.6, 48.5, 48.4, 47.0, 19.2, 18.1, 15.2; HRMS (ESI/FTICR) *m/z*; $[M + H]^+$ Calcd for $C_{73}H_{75}N_8O_8^+$ 1191.5630; Found 1191.5650.

Cyclo-(*N*spe$_2$-*N*pm$_2$)$_2$ (**35**): white amorphous solid, 0.061 g, 33% yield; t_R: 16.1 min. ^{1}H NMR (600 MHz, $CDCl_3$, complex mixture of rotamers) δ: 7.40-7.03 (40H, overlapping, Ar-*H*), 4.27-3.37 (28H, overlapping, N-C*H*CH$_3$-Ph, N-C*H*$_2$-Ph, O=C-C*H*$_2$-N-CH$_2$-Ph, O=C-C*H*$_2$-N-CHCH$_3$-Ph), 1.46-0.99 (12H, overlapping, N-CHC*H*$_3$-Ph); ^{13}C{^{1}H} NMR (150 MHz, $CDCl_3$, complex mixture of rotamers) δ: 170.6, 170.1, 169.8, 169.7, 169.6, 168.7, 168.1, 167.6, 167.5, 167.1, 166.2, 141.2, 141.0, 140.7, 140.6, 140.2, 137.9, 136.8, 136.6, 136.4, 136.1, 135.8, 135.3, 134.9, 129.1, 129.0, 128.9, 128.8, 128.7, 128.5, 128.0, 127.9, 127.8, 127.5, 127.3, 127.1, 126.8, 126.6, 126.5, 126.4, 126.2, 126.1, 126.0, 125.7, 56.2, 54.9, 54.5, 54.1, 53.4, 53.0, 52.6, 52.4, 52.2, 51.9, 51.7, 51.5, 51.1, 50.9, 50.7, 50.3, 50.2, 49.8, 49.6, 49.3, 49.0, 48.5, 48.3, 48.1, 47.9, 47.6, 47.4, 46.6, 46.5, 45.8, 45.3, 44.7, 44.5, 44.3, 44.0, 43.8, 43.2, 19.0, 18.4, 18.2, 17.5, 17.3, 16.8, 16.5, 16.3, 15.7, 15.1, 15.0, 14.6; HRMS (ESI/FTICR) *m/z*; $[M + H]^+$ Calcd for $C_{76}H_{81}N_8O_8^+$ 1233.6172; Found 1233.6153.

Cyclo-{[(*cis*,$_p$*R*)*N*spe-(*cis*,$_p$*S*)*N*spe-(*trans*,$_p$*S*)*N*spe-(*trans*,$_p$*R*)*N*spe]$_2$} (**36**): white amorphous solid, 0.104 g, 54% yield; t_R: 16.6 min. ^{1}H NMR (600 MHz, $C_6D_5CD_3$, mixture of conformational isomers with 62% of *ccttcctt*-**36**) δ: 7.55 (4H, d, *J* 7.7 Hz, Ar-*H*), 7.19-7.03 (32H, overlapping, Ar-*H*), 6.58 (4H, d, *J* 7.4 Hz, Ar-*H*), 6.14 (2H, q, *J* 6.9 Hz, N$_c$-C*H*CH$_3$-Ph), 5.47 (2H, q, *J* 7.0 Hz, N$_c$-C*H*CH$_3$-Ph), 4.55 (2H, d, *J* 16.9 Hz, O=C-C*H*H-N$_t$-CHCH$_3$-Ph), 4.44 (2H, d, *J* 18.0 Hz, O=C-C*H*H-N$_c$-CHCH$_3$-Ph), 4.40 (2H, q, *J* 6.8 Hz, N$_t$-C*H*CH$_3$-Ph), 4.22 (2H, q, *J* 6.8 Hz, N$_t$-C*H*CH$_3$-Ph), 4.09 (2H, d, *J* 16.5 Hz, O=C-C*H*H-N$_t$-CHCH$_3$-Ph), 3.65 (4H, br d, overlapping, O=C-CH*H*-N$_t$-CHCH$_3$-Ph and O=C-CH*H*-N$_c$-CHCH$_3$-Ph), 3.58 (2H, d, *J* 17.7 Hz, O=C-C*H*H-N$_c$-CHCH$_3$-Ph), 3.32 (2H, d, *J* 17.7 Hz, O=C-CH*H*-N$_c$-CHCH$_3$-Ph), 3.21 (2H, d, *J* 16.5 Hz, O=C-CH*H*-N$_t$-CHCH$_3$-Ph), 1.66 (6H, d, *J* 6.9 Hz, N$_c$-CHC*H*$_3$-Ph), 1.54 (6H, d, *J* 6.8 Hz, N$_t$-CHC*H*$_3$-Ph, *t*), 1.46 (6H, d, *J* 6.8 Hz, N$_t$-CHC*H*$_3$-Ph), 1.00 (6H, d, *J* 7.0 Hz, N$_c$-CHC*H*$_3$-Ph); ^{13}C{^{1}H} NMR (150 MHz, $C_6D_5CD_3$, mixture of conformational isomers with 62% of *ccttcctt*-**36**; due to the presence of further

conformational isomers, the spectrum was assigned also on the basis of the HSQC and HMBC experiments) δ: 170.5 (x2), 168.9 (x2), 167.7 (x2), 167.2 (x2), 141.3 (x2), 140.8 (x2), 139.9 (x2), 139.2 (x2), 129.5-127.4 (x40 C-H signals aromatic overlapping with $C_6D_5CD_3$ signals), 55.8 (x2), 55.2 (x2), 54.2 (x2), 54.1 (x2), 47.2 (x2), 46.6 (x2), 45.1 (x2), 44.8 (x2), 18.8 (x2), 17.6 (x2), 17.4 (x2), 16.9 (x2). HRMS (ESI/FTICR) *m/z*; $[M + H]^+$ Calcd for $C_{80}H_{89}N_8O_8^+$ 1289.6798; Found 1289.6817.

*General procedure for the Na^+ complexes formation [**28a**,**30a**,**35a/b**,**36a**·nNa]$^{n+}$ n[TFPB]$^-$, and [**36b**·Na]$^+PF_6^-$.* To a solution of cyclic hexameric or octameric peptoids in $CDCl_3$ or $CDCl_3$:CD_3CN = 9:1 (1.0 mL) increasing quantities of NaTFPB or $NaPF_6$ were added. After the addition the mixtures were sonicated for 5 minutes in a r.t. bath (25 °C) and the requested NMR spectra were acquired.

[**28a**·Na]$^+$[TFPB]$^-$: white amorphous solid. ^{1}H-NMR (600 MHz, $CDCl_3$) δ: 7.71 (8H, s, TFPB-*o*-*H*), 7.51 (4H, s, TFPB-*p*-*H*), 7.34-7.29 (18H, br signals, overlapping, Ar-*H*), 6.99 (6H, m, Ar-*H*), 6.92 (6H, m, Ar-*H*), 4.94 (3H, q, *J* 6.8 Hz, N-C*H*CH_3-Ph), 4.87 (3H, d, *J* 16.8 Hz, O=C-C*H*H-N-CH_2-Ph), 4.64 (3H, d, *J* 16.0 Hz, N-C*H*H-Ph), 4.57 (3H, d, *J* 17.3 Hz, O=C-C*H*H-N-$CHCH_3$-Ph), 4.37 (3H, d, *J* 16.0 Hz, N-CH*H*-Ph), 3.68 (3H, d, *J* 16.8 Hz, O=C-CH*H*-N-CH_2-Ph), 3.44 (3H, d, *J* 17.3 Hz, O=C-CH*H*-N-$CHCH_3$-Ph), 1.56 (9H, br d, N-CHC*H*$_3$-Ph). ESI-MS *m/z* 947.8 $[M + Na]^+$.

[**28a**·2Na]$^{2+}$2[TFPB]$^-$: white amorphous solid. ^{1}H-NMR (600 MHz, $CDCl_3$) δ: 7.71 (16H, s, TFPB-*o*-*H*), 7.52 (8H, s, TFPB-*p*-*H*), 7.33-7.32 (18H, br signals, overlapping, Ar-*H*), 6.99 (6H, m, Ar-*H*), 6.92 (6H, m, Ar-*H*), 4.93 (3H, q, *J* 6.8 Hz, N-C*H*CH_3-Ph), 4.77 (3H, d, *J* 16.8 Hz, O=C-C*H*H-N-CH_2-Ph), 4.59 (3H, d, *J* 16.0 Hz, N-C*H*H-Ph), 4.37 (3H, d, *J* 17.3 Hz, O=C-C*H*H-N-$CHCH_3$-Ph), 4.27 (3H, d, *J* 16.0 Hz, N-CH*H*-Ph), 3.75 (3H, d, *J* 16.8 Hz, O=C-CH*H*-N-CH_2-Ph), 3.43 (3H, d, *J* 17.3 Hz, O=C-CH*H*-N-$CHCH_3$-Ph), 1.40 (9H, d, *J* 6.8 Hz, N-CHC*H*$_3$-Ph); ^{13}C{^{1}H} NMR (150 MHz, $CDCl_3$) δ: 169.9 (x3), 168.1 (x3), 161.7 (q, *J* 50 Hz, TFPB: C_{Ar}-B), 137.1 (x3), 134.8 (TFPB: C_o-H), 133.1 (x3), 129.3 (x10), 128.9 (q, *J* 30 Hz, TFPB: $\underline{C}_m$-CF_3), 126.9 (x10), 126.0 (x10), 124.6 (q, *J* 270 Hz, TFPB: CF_3), 117.6 (TFPB: C_p-H), 55.6 (x3), 53.5 (x3), 49.7 (x3), 44.9 (x3), 16.8 (x3). ESI-MS *m/z* 947.7 $[M + Na]^+$.

[**30a**·Na]$^+$[TFPB]$^-$: white amorphous solid. ^{1}H-NMR (400 MHz, $CDCl_3$) δ: 7.71 (8H, s, TFPB-*o*-*H*), 7.50 (4H, s, TFPB-*p*-*H*), 7.38 (12H, br s, Ar-*H*), 7.28 (6H, br s, Ar-*H*), 6.68 (6H, d, *J* 7.3 Hz, Ar-*H*), 5.00 (3H, q, *J* 6.6 Hz, N-C*H*CH_3-Ph), 4.87 (3H, q, *J* 6.6 Hz, N-C*H*CH_3-Ph), 4.60 (3H, d, *J* 16.8 Hz, O=C-C*H*H-N-$CHCH_3$-Ph), 4.52 (3H, d, *J* 16.9 Hz, O=C-C*H*H-N-$CHCH_3$-Ph), 3.62 (3H, d, *J* 16.8 Hz, O=C-CH*H*-N-$CHCH_3$-Ph), 3.38 (3H, d, *J* 16.9 Hz, O=C-CH*H*-N-$CHCH_3$-Ph), 1.53 (9H, d, *J* 6.6 Hz, N-CHC*H*$_3$-Ph), 1.49 (9H, d, *J* 6.6 Hz, N-CHC*H*$_3$-Ph). ESI-MS *m/z* 989.7 [M + Na]$^+$.

[**30a**·2Na]$^+$2[TFPB]$^-$: white amorphous solid. ^{1}H-NMR (600 MHz, $CDCl_3$) δ: 7.71 (16H, s, TFPB-*o*-*H*), 7.51 (8H, s, TFPB-*p*-*H*), 7.32-7.22 (18H, br signals, overlapping, Ar-*H*), 7.13 (6H, d, *J* 7.5 Hz, Ar-*H*), 6.73 (6H, d, *J* 7.5 Hz, Ar-*H*), 4.91 (6H, q, *J* 6.7 Hz, N-C*H*CH_3-Ph), 4.51 (3H, d, *J* 16.5 Hz, O=C-C*H*H-N-$CHCH_3$-Ph), 4.30 (3H, d, *J* 17.2 Hz, O=C-C*H*H-N-$CHCH_3$-Ph), 3.76 (3H, d, *J* 16.5 Hz, O=C-CH*H*-N-$CHCH_3$-Ph), 3.34 (3H, d, *J* 17.2 Hz, O=C-CH*H*-N-$CHCH_3$-Ph), 1.46 (9H, d, *J* 6.7 Hz, N-CHC*H*$_3$-Ph), 1.38 (9H, d, *J* 6.7 Hz, N-CHC*H*$_3$-Ph); ^{13}C{^{1}H} NMR (150 MHz, $CDCl_3$) δ: 168.4 (x3), 167.9 (x3), 161.7 (q, *J* 50 Hz, TFPB: C_{Ar}-B), 137.4 (x3), 136.1 (x3), 134.8 (TFPB: C_o-H), 129.5 (x6), 128.8 (q, *J* 30 Hz, TFPB: $\underline{C}_m$-CF_3), 129.5 (x12), 127.5 (x6), 125.7 (x6), 124.6 (q, *J* 270 Hz, TFPB: CF_3), 117.4 (TFPB: C_p-H), 56.2 (x3), 55.1 (x3), 44.2 (x3), 45.0 (x3), 18.2 (x3), 16.5 (x3). ESI-MS *m/z* 989.9 [M + Na]$^+$.

[**35a**·2Na]$^{2+}$2[TFPB]$^-$/[**35b**·2Na]$^{2+}$2[TFPB]$^-$: white amorphous solid. ^{1}H-NMR (600 MHz, $CDCl_3$, 50:50 mixture of conformational isomers) δ: 7.72 (16H, s, TFPB-*o*-*H*), 7.52 (8H, s, TFPB-*p*-*H*), 7.33-7.12 (28H, br signals, overlapping, Ar-*H*), 6.97-6.94 (4H, br signals, overlapping, Ar-*H*), 6.88 (2H, d, *J* 7.1 Hz, Ar-*H*), 6.77 (2H, d, *J* 7.3 Hz, Ar-*H*), 6.57 (2H, d, *J* 7.5 Hz, Ar-*H*), 6.45 (2H, d, *J* 7.7 Hz, Ar-*H*), 5.12 (1H, d, *J* 7.2 Hz, O=C-C*H*H-N-CH_2-Ph), 5.09 (1H, d, *J* 7.4 Hz, O=C-C*H*H-N-CH_2-Ph), 4.99 (1H, q, *J* 6.9 Hz, N-C*H*CH_3-Ph), 4.95 (1H, q, *J* 7.0 Hz, N-C*H*CH_3-Ph), 4.93-4.90 (2H, overlapping, N-C*H*CH_3-Ph and O=C-C*H*H-N-CH_2-Ph), 4.82 (1H, d, *J* 17.3 Hz, O=C-C*H*H-N-$CHCH_3$-Ph), 4.79 (1H, q, *J* 6.8 Hz, N-C*H*CH_3-Ph), 4.67 (1H, d, *J* 18.2 Hz, O=C-C*H*H-N-CH_2-Ph), 4.64 (1H, d, *J* 16.6 Hz, O=C-C*H*H-N-$CHCH_3$-Ph), 4.63 (1H, d, *J* 16.7 Hz, N-C*H*H-Ph), 4.53-4.47 (1H, O=C-CH*H*-N-$CHCH_3$-Ph and 3H, N-C*H*H-Ph, overlapping),

4.33 (1H, d, *J* 16.8 Hz, O=C-C*H*H-N-CHCH$_3$-Ph), 4.14 (1H, d, *J* 16.5 Hz, N-CH*H*-Ph), 4.06 (1H, d, *J* 16.3 Hz, N-CH*H*-Ph), 4.01 (1H, d, *J* 16.3 Hz, N-CH*H*-Ph), 3.95 (1H, d, *J* 16.7 Hz, N-CH*H*-Ph), 3.75-3.71 (4H, overlapping d, O=C-CH*H*-N-CH$_2$-Ph, O=C-CH*H*-N-CHCH$_3$-Ph and O=C-C*H*H-N-CHCH$_3$-Ph), 3.67 (1H, d, *J* 10.7 Hz, O=C-CH*H*-N-CH$_2$-Ph), 3.64 (1H, d, *J* 10.2 Hz, O=C-CH*H*-N-CHCH$_3$-Ph), 3.45 (1H, d, *J* 18.2 Hz, O=C-CH*H*-N-CH$_2$-Ph), 3.34 (1H, d, *J* 16.8 Hz, O=C-CH*H*-N-CH$_2$-Ph), 1.46 (3H, d, *J* 6.9 Hz, N-CHC*H*$_3$-Ph), 1.44 (3H, d, *J* 6.9 Hz, N-CHC*H*$_3$-Ph), 1.36 (3H, d, *J* 7.0 Hz, N-CHC*H*$_3$-Ph), 1.28 (3H, d, *J* 6.8 Hz, N-CHC*H*$_3$-Ph); ^{13}C{^{1}H} NMR (150 MHz, $CDCl_3$) δ: 170.2, 170.0, 169.6, 169.1, 169.0, 168.8, 168.2, 167.9, 161.7 (q, *J* 50 Hz, TFPB: C_{Ar}-B), 137.7 (x2), 135.4 (x2), 134.8 (TFPB: C_o-H), 133.1 (x2), 132.8 (x2), 129.4 (x8), 129.3 (x8), 128.8 (q, *J* 30 Hz, TFPB: $\underline{C}_m$-CF_3), 128.0 (x8), 126.7 (x8), 126.5 (x4), 125.6 (x4), 124.6 (q, *J* 270 Hz, TFPB: CF_3), 117.4 (TFPB: C_p-H), 55.7 (x2), 55.5, 55.0, 51.7 (x2), 51.4 (x2), 47.8 (x2), 47.6, 47.3, 46.9, 44.8, 44.3, 44.1, 18.0, 17.7, 17.5 (x2). ESI-MS *m/z* 1256.0 $[M + Na]^+$.

[**36a**·2Na]$^{2+}$2[TFPB]$^-$: white amorphous solid. ^{1}H-NMR (600 MHz, $CDCl_3$) δ: 7.71 (16H, s, TFPB-*o*-*H*), 7.52 (8H, s, TFPB-*p*-*H*), 7.38-7.27 (24H, br signals, overlapping, Ar-*H*), 7.12 (8H, d, *J* 7.5 Hz, Ar-*H*), 6.57 (8H, d, *J* 7.5 Hz, Ar-*H*), 4.84 (8H, q, *J* 6.9 Hz, N-C*H*CH$_3$-Ph), 4.58 (4H, d, *J* 16.7 Hz, O=C-C*H*H-N-CHCH$_3$-Ph), 4.42 (4H, d, *J* 16.8 Hz, O=C-C*H*H-N-CHCH$_3$-Ph), 3.70 (4H, d, *J* 16.7 Hz, O=C-CH*H*-N-CHCH$_3$-Ph), 3.46 (4H, d, *J* 16.8 Hz, O=C-CH*H*-N-CHCH$_3$-Ph), 1.36 (12H, d, *J* 6.9 Hz, N-CHC*H*$_3$-Ph), 1.34 (12H, d, *J* 6.9 Hz, N-CHC*H*$_3$-Ph); ^{13}C{^{1}H} NMR (150 MHz, $CDCl_3$) δ: 169.2 (x4), 168.4 (x4), 161.7 (q, *J* 50 Hz, TFPB: C_{Ar}-B), 137.9 (x4), 135.5 (x4), 134.8 (TFPB: C_o-H), 129.5 (x8), 129.2 (x8), 129.0 (x8), 128.8 (q, *J* 30 Hz, TFPB: $\underline{C}_m$-CF_3), 128.2 (x8), 125.5 (x8), 124.6 (q, *J* 270 Hz, TFPB: CF_3), 117.4 (TFPB: C_p-H), 55.6 (x4), 55.0 (x4), 44.5 (x4), 44.2 (x4), 18.0 (x4), 17.4 (x4). ESI-MS *m/z* 1312.1 $[M + Na]^+$.

[**36b**·Na]$^+PF_6^-$: white amorphous solid. ^{1}H-NMR (600 MHz, $CDCl_3$:CD_3CN = 9:1) δ: 7.33-7.25 (32H, overlapping, Ar-*H*), 7.16-7.13 (8H, overlapping, Ar-*H*), 6.04 (4H, q, *J* 7.1 Hz, N$_c$-C*H*CH$_3$-Ph), 4.81 (4H, q, *J* 7.0 Hz, N$_t$-C*H*CH$_3$-Ph), 4.75 (4H, d, *J* 16.6 Hz, O=C-C*H*H-N$_t$-CHCH$_3$-Ph), 3.86 (4H, d, *J* 18.0 Hz, O=C-C*H*H-N$_c$-CHCH$_3$-Ph), 3.59 (4H, d, *J* 18.0 Hz, O=C-CH*H*-N$_c$-CHCH$_3$-Ph), 3.21 (4H, d, *J* 16.6 Hz,

O=C-CH*H*-N$_c$-CHCH$_3$-Ph), 1.62 (12H, d, *J* 7.0 Hz, N$_t$-CHC*H*$_3$-Ph), 1.57 (12H, d, *J* 7.1 Hz, N$_c$-CHC*H*$_3$-Ph); ^{13}C{^{1}H} NMR (150 MHz, $CDCl_3$:CD_3CN = 9:1) δ: 168.8 (x4), 168.1 (x4), 140.8 (x4), 140.0 (x4), 128.7 (x10), 128.3 (x10), 127.2 (x10), 125.8 (x10), 55.1 (x4), 51.8 (x4), 45.8 (x4), 43.1 (x4), 18.2 (x4), 15.6 (x4). ESI-MS *m/z* 1311.2 $[M + Na]^+$.

*General procedure for evaluation of $K_{a1/2}$ in [**28a**, **30a**·Na]$^+$ [TFPB]$^-$, [**35a/b**, **36a**·2Na]$^{2+}$ 2[TFPB]$^-$, [**36b**·Na]$^+PF_6^-$. (a) Evaluation of the apparent K_{a1} in [**28a**, **30a**·Na]$^+$[TFPB]$^-$*: To a solution of hexameric cyclic peptoids **28** or **30** in $CDCl_3$ (0.5 mL, 3.0 mM) 1.0 equivalent of NaTFPB (3.0 mM) was added. After the addition the mixture was sonicated for 5 minutes (25 °C). The H·G complex concentration, at the equilibrium – $[H{\cdot}G]_{eq}$ – was evaluated by integration of the ^{1}H NMR complex signals (2.5-6.5 range) versus the total integration of the free host plus complexed molecules at 298 K. With the addition of 1 equivalent of guest, the equilibrium (1) is established:

$$H + G \rightleftharpoons H{\cdot}G \qquad (1)$$

Equation (2) was used to obtain the concentration of the $[H{\cdot}G]_{eq}$ species.

$$[H{\cdot}G]_{eq} = \frac{F_a}{F_b} \times [C]_i \qquad (2)$$

Where F_a and F_b are the areas of the signals of the host/guest adduct and host plus host/guest adduct, respectively (recorded in the 2.5-6.5 range); $[C]_i$ is the host initial concentration (3.0 mM).

In the case of the formation of a monosodium complex, the evaluation of the concentration of the species, at the equilibrium, follows the relation (3):

$$[H]_{eq} = [G]_{eq} = [H]_i - [H{\cdot}G]_{eq} \qquad (3)$$

The apparent K_{a1}, was calculated following (4):

$$K_{a1} = \frac{[H{\cdot}G]_{eq}}{[H]_{eq} \times [G]_{eq}} \qquad (4)$$

In order to have reliable integration values, the delay times (D1) among successive scans, in the ^{1}H NMR, were set at 5 seconds.

*(b) Evaluation of the apparent K_{a2} in [**35a/b**, **36a**·2Na]$^{2+}$ 2[TFPB]$^-$*: To a solution of cyclic peptoids **35** or **36** in $CDCl_3$ (0.5 mL, 3.0 mM) 2.0 equivalents of NaTFPB were added (6.0 mM). After the addition the mixture was sonicated for 5 minutes (25 °C). The $H{\cdot}G_2$ complex concentration, at the equilibrium – $[H{\cdot}G_2]_{eq}$ – was evaluated by integration of the ^{1}H NMR complex signals (2.5-6.5 range) versus the total integration of the free host plus complexed molecules at 298 K. With the addition of 2 equivalents of guest, the equilibrium (5) is established:

$$H + 2\,G \rightleftharpoons H{\cdot}G_2 \qquad (5)$$

$$[H]_{eq} = [H]_i - [H{\cdot}G_2]_{eq} \qquad (6)$$

$$[G]_{eq} = [G]_i - 2[H{\cdot}G_2]_{eq} \qquad (7)$$

(where $[G]_i = 2[H]_i$).

The K_{aTOT} (= $K_{a1}{\cdot}K_{a2}$, where K_{a1} is the equilibrium constant associated with the formation of the monometallic complex, K_{a2} is the equilibrium constant associated with the formation of the bimetallic complex), was calculated as follows:

$$K_{aTOT} = \frac{[H{\cdot}G_2]_{eq}}{[H]_{eq} \times [G]^2_{eq}} \qquad (8)$$

for the equilibrium (5).

In order to have reliable integration values, the delay times (D1) among successive scans, in the ^{1}H NMR, were set at 5 seconds. Note that for [**35a/b**·2Na]$^{2+}$ the K_a is referred to the sum of both the complexes.

(c) Evaluation of the apparent K_{a1} in [36b·Na]$^+PF_6^-$: To a solution of octameric cyclic peptoid **36** in $CDCl_3$ (0.45 mL, 3.0 mM) a solution of $NaPF_6$ in CD_3CN (1.0 equivalent, 0.05 mL, 3.0 mM) was added. After the addition the mixture was sonicated for 5 minutes (25 °C). As in paragraph 1.4.1, the H·G complex concentration, at the equilibrium – $[H·G]_{eq}$ – was evaluated by integration of the ^{1}H NMR complex signals (2.5-6.5 range) versus the total integration of the free host plus the complexed molecule at 298 K.

The calculations follow exactly the same procedure seen for [**28a**, **30a**·Na]$^+$[TFPB]$^-$.

Computational Methodology. The DFT calculations were performed with the Gaussian09 set of programs,[33] using the BP86 functional of Becke and Perdew.[34] The electronic configuration of the molecular systems was described with the standard triple zeta valence basis set with a polarization function of Ahlrichs and co-workers for H, C, N, O, Na (TZVP keyword in Gaussian).[35] The geometry optimizations were performed without symmetry constraints, and the characterization of the located stationary points was performed by analytical frequency calculations. Solvent effects including contributions of non-electrostatic terms have been estimated in single-point calculations on the gas phase optimized structures, based on the polarizable continuous solvation model PCM using DMSO or $CHCl_3$ as a solvent.[36]

X-ray Crystallography. Colorless needle-like crystals of compound **15** suitable for X-ray diffraction analysis were obtained by slow evaporation, dissolving 3 mg of the compound in 1.0 mL of ethyl acetate. Colorless needle-like single crystals of compound **16** were obtained by slow evaporation of a solution of compounds **16**/**17** (5 mg) in 1.2 mL hot dichloromethane. Colorless needle-like single crystals of compound **19** were obtained by slow evaporation of a solution of chloroform/toluene (2:1), dissolving 5 mg of the compound in 0.4 mL of chloroform and adding 0.2 mL of toluene. Colorless needle-like single crystals of compound **30** suitable for X-ray diffraction analysis were obtained by slow evaporation of a

solution of ethyl acetate/diethyl ether (2:1) dissolving 5 mg of the compound in 1.6 mL of hot ethyl acetate and adding 0.8 mL of diethyl ether. Colorless needle-like single crystals of compound [**36b**·Na(H_2O)]$^+$[PF_6]$^-$·0.25(CH_3CN) suitable for X-ray diffraction analysis were obtained by slow evaporation, dissolving 3 mg of the compound **36** and 1 eq of $NaPF_6$ in 1.2 mL of hot acetonitrile.

In all cases a suitable crystal was selected and mounted on a cryoloop with paratone oil and measured at room temperature with a Bruker D8 QUEST diffractometer equipped with a PHOTON II detector using Cu$K\alpha$ radiation (λ= 1.54178 Å). Indexing was performed using APEX3.[37] Data integration and reduction were performed using SAINT.[37] Absorption correction was performed by multi-scan method in SADABS.[37] The structures were solved using SIR2014[38] and refined by means of full matrix least-squares based on F^2 using the program SHELXL.[39] For all compounds non-hydrogen atoms were refined anisotropically. For compound **15** hydrogen atoms (except hydroxyl hydrogen atom) were positioned geometrically and included in structure factors calculations, but not refined. Hydroxyl hydrogen atom was located in the Fourier difference map and refined isotropically. For compounds **16** and **30** all hydrogen atoms were positioned geometrically and included in structure factors calculations, but not refined. In compound **19** one chiral side chain shows two possible positions with refined occupancy factors 0.531(15) and 0.469(15). Thus, restraints on anisotropic displacement parameters were applied to disordered group atoms. As for compound [**36b**·Na(H_2O)]$^+$[PF_6]$^-$·0.25(CH_3CN), the disordered PF_6^- groups were refined as rigid bodies considering that they are inclined with respect to the fourfold axes. Isotropic displacement parameters were used for disordered PF_6^- anion atoms. Residual acetonitrile solvent molecules were located in final difference Fourier maps and refined by fixing their occupancy factors to 0.25 and considering a global isotropic displacement factor. Crystallographic data and refinement details for the compounds are listed in Table S4. ORTEP diagrams were drawn using OLEX2[40] and are shown in Figures S33-S37.

ASSOCIATED CONTENTS

J. Org. Chem. 2019, 84, 17, 10911−10928 DOI: 10.1021/acs.joc.9b01509

Supporting Information

The Supporting Information is available free of charge on the ACS Publications website. Procedures for the evaluation of the apparent K_{a1} in [**28a**, **30a**·Na]$^+$[TFPB]$^-$, [**36b**·Na]$^+$$PF_6^-$, and K_{a2} in [**35a**/**b**, **36a**·2Na]$^{2+}$2[TFPB]$^-$. 1D and 2D spectra of cyclic 1D and 2D spectra of cyclic derivatives **1**/**2**, **8**, **9**, **16**/**17**, **19**, **27**, **28**, **30**, **34**, **35**, **36** and their complexes. ^{1}H NMR at variable temperature and titration experiments, HPLC chromatograms of linear and cyclic peptoids. Minimum energy structures and cartesian coordinates of **1**, **2**, **5**, **9**, **16**, **17**, **19**, **20**, **28**, **29**, **36**, **37**, [**28a**·Na]$^+$, [**28b**·Na]$^+$, [**30a**·Na]$^+$. X-ray crystallographic data for **15**, **16**, **19**, **30**, [**36b**·Na(H_2O)]$^+$[PF_6]$^-$·0.25(CH_3CN) (CIF).

AUTHOR INFORMATION

Corresponding Authors

*dericca@unisa.it

*ccostabile@unisa.it

ORCID

Assunta Amato: 0000-0001-9246-5523

Giovanni Pierri: 0000-0001-5433-6077

Consiglia Tedesco: 0000-0001-6849-798X

Giorgio Della Sala: 0000-0001-5020-8502

Irene Izzo: 0000-0002-0369-0102

Chiara Costabile: 0000-0001-8538-7125

Francesco De Riccardis: 0000-0002-8121-9463

Author Contributions

The manuscript was written through contributions of all authors. All authors have given approval to the final version of the manuscript.

Notes

The authors declare no competing financial interest.

ACKNOWLEDGEMENTS

Financial support from the University of Salerno (FARB), and from POR CAMPANIA FESR 2007/2013 O.O.2.1.-CUP B46D14002660009 "Il potenziamento e la riqualificazione del sistema delle infrastrutture nel settore dell'istruzione, della formazione e della ricerca". We thank Patrizia Iannece for HR-MS and elemental analysis, and Patrizia Oliva for NMR spectra.

REFERENCES AND NOTES

[1] a) Gellman, S. H. Foldamers: A Manifesto. *Acc. Chem. Res*. **1998**, *31*, 173–180; b) Hill, D. J.; Mio, M. J.; Prince, R. B.; Hughes, T. S.; Moore, J. S. A Field Guide to Foldamers. *Chem. Rev*. **2001**, *101*, 3893–4011; c) Le Bailly, B. A. F.; Clayden, J. Dynamic foldamer chemistry. *Chem.Commun*. **2016***, 52*, 4852–4863.

[2] a) Yoo, B.; Kirshenbaum K. Peptoid architectures: elaboration, actuation, and application. *Curr. Opin. Chem. Biol.* **2008**, *12*, 714–721; b) Maayan, G. Conformational Control in Metallofoldamers: Design, Synthesis and Structural Properties. *Eur. J. Org. Chem.* **2009**, 5699–5710; c) D'Amato, A.; Schettini, R.; Della Sala, G.; Costabile, C.; Tedesco, C.; Izzo, I.; De Riccardis, F. Conformational isomerism in cyclic peptoids and its specification. *Org. Biomol. Chem.* **2017**, *15*, 9932–9942; d) Sun, J.; Zuckermann, R. N. Peptoid Polymers: A Highly Designable Bioinspired Material. *ACS Nano* **2013**, *7*, 4715–4732; e) Dale, J.; Titlestad, K. Conformational Processes in Simple Cyclic Peptides. *Acta Chem. Scand. B*, **1975**, *29*, 353–361.

[3] a) Fowler, S. A.; Blackwell, H. E. Structure–function relationships in peptoids: Recent advances toward deciphering the structural requirements for biological function, *Org. Biomol. Chem.* **2009**, *7*, 1508–1524; b) D'Amato, A.; Volpe, R.; Vaccaro, M. C.; Terracciano, S.; Bruno, I.; Tosolini, M.; Tedesco, C.; Pierri, G.; Tecilla, P.; Costabile, C.; Della Sala, G.; Izzo, I.; De Riccardis, F. Cyclic Peptoids as Mycotoxin Mimics: An Exploration of Their Structural and Biological Properties. *J. Org. Chem.* **2017**, *82*, 8848**–**8863; c) D'Amato, A.; Della Sala, G.; Izzo, I.; Costabile, C.; Masuda, Y.; De Riccardis, F. Cyclic Octamer Peptoids: Simplified Isosters of Bioactive Fungal Cyclodepsipeptides. *Molecules* **2018**, *23*, 1779.

[4] a) Armand, P.; Kirshenbaum, K.; Goldsmith, R. A.; Farr-Jones, S.; Barron, A. E.; Truong, K. T. V.; Dill, K. A.; Mierke, D. F.; Cohen, F. E.; Zuckermann, R. N.; Bradley, E. K. NMR determination of the major solution conformation of a peptoid pentamer with chiral side chains. *Proc. Natl. Acad. Sci. USA* **1998**, *95*, 4309–4314; b) Szekely, T.; Caumes, C.; Roy, O.; Faure, S.; Taillefumier, C. α-Peptoïdes Et Composés Apparentés: Synthèse Et Contrôle De La Conformation (α-Peptoids and Related Compounds: Synthesis and Control of the Conformation). *C. R. Chimie* **2012**, *16*, 318–330. c) Butterfoss, G. L.; Yoo, B.; Jaworski, J. N.; Chorny, I.; Dill, K. A.; Zuckermann, R. N.; Bonneau, R.; Kirshenbaum, K.; Voelz, V. A. De novo structure prediction and experimental characterization of folded peptoid oligomers. *Proc. Natl. Acad. Sci. USA* **2012**, *109*, 14320–14325; d) Roy, O.; Dumonteil, G.; Faure, S.; Jouffret, L.; Kriznik, A.; Taillefumier, C. Homogeneous and Robust Polyproline Type I Helices from Peptoids with Nonaromatic α-Chiral Side Chains. *J. Am. Chem. Soc*. **2017**, *139*, 13533−13540. e) Roy, O.; Caumes, C.; Esvan, Y.; Didierjean, C.; Faure, S.; Taillefumier C. The *tert*-Butyl Side Chain: A Powerful Means to Lock Peptoid Amide Bonds in the Cis Conformation. *Org. Lett*. **2013**, *15*, 2246−2249.

[5] a) Webster, A. M.; Cobb, S. L. Recent Advances in the Synthesis of Peptoid Macrocycles. *Chem. Eur. J.* **2018**, *24*, 7560–7573; b) Yoo, B.; Shin, S. B. Y.; Huang, M. L.; Kirshenbaum, K. Peptoid Macrocycles: Making the Rounds with Peptidomimetic Oligomers. *Chem. Eur. J.* **2010**, *16*, 5528–5537; c) Shin, S. B. Y.; Yoo, B.; Todaro, L. J.; Kirshenbaum, K. Cyclic Peptoids. *J. Am. Chem. Soc.* **2007**, *129*,

3218–3225. d) Tedesco, C.; Erra, L.; Izzo, I.; De Riccardis, F. Solid state assembly of cyclic α-peptoids. *CrystEngComm.* **2014**, *16*, 3667–3687.

[6] Maayan, G.; Albrecht, M. (Eds.) in *Metallofoldamers. Supramolecular Architectures from Helicates to Biomimetic;* John Wiley & Sons, Chichester, 2013.

[7] a) Crapster, J. A.; Guzei, I. A.; Blackwell, H. E. A Peptoid Ribbon Secondary Structure. *Angew. Chem. Int. Ed.* **2013***, 52*, 5079–5084; b) Gorske, B. C.; Stringer, J. R.; Bastian, B. L.; Fowler, S. A.; Blackwell, H. E. New Strategies for the Design of Folded Peptoids Revealed by a Survey of Noncovalent Interactions in Model Systems. *J. Am. Chem. Soc.* **2009**, *131*, 16555–16567; c) Gorske, B. C.; Nelson, R. C.; Bowden, Z. S.; Kufe, T. A.; Childs, A. M. "Bridged" n→π* Interactions Can Stabilize Peptoid Helices. *J. Org. Chem.* **2013**, *78*, 11172−11183; d) D'Amato, A.; Pierri, G.; Costabile, C.; Della Sala, G.; Tedesco, C.; Izzo, I.; De Riccardis, F. Cyclic Peptoids as Topological Templates: Synthesis via Central to Conformational Chirality Induction. *Org. Lett*. **2018**, *20*, 640−643; e) Wu, C. E.; Kirshenbaum, K.; Sanborn, T. J.; Patch, J. A.; Huang, K.; Dill, K. A.; Zuckermann, R. N.; Barron, A. Structural and Spectroscopic Studies of Peptoid Oligomers with α-Chiral Aliphatic Side Chains. *J. Am. Chem. Soc.* **2003**, *125*, 13525–13530; f) Mannige, R. V.; Haxton, T. K.; Proulx, C.; Robertson, E. J.; Battigelli, A.; Butterfoss, G. L.; Zuckermann, R. N.; Whitelam, S. Peptoid nanosheets exhibit a new secondary-structure motif. *Nature* **2015**, *526*, 415–420.

[8] Newberry, R. W.; Raines, R. T. The n→π* Interaction. *Acc. Chem. Res.* **2017**, *50*, 1838–1846.

[9] Hoffmann, R. W. Allylic 1,3-strain as a controlling factor in stereoselective transformations. *Chem. Rev*. **1989**, *89*, 1841−1860.

[10] a) Bhattacharyya, R.; Chakrabarti, P. Stereospecific interactions of proline residues in protein structures and complexes. *J. Mol. Biol*. **2003**, *331*, 925−940; b) Guo, H.; Beahm, R. F.; Guo, H. Stabilization and Destabilization of the C^{δ}−H···OC Hydrogen Bonds Involving Proline Residues in Helices. *J. Phys. Chem. B* **2004**, *108*, 18065−18072; c) Gimenez, D.; Aguilar, J. A.; Bromley, E. H. C.; Cobb, S. L.

Stabilising Peptoid Helices Using Non-Chiral Fluoroalkyl Monomers. *Angew. Chem. Int. Ed.* **2018**, *57*, 10549–10553.

[11] Armand, P.; Kirshenbaum, K.; Falicov, A.; Dunbrack, R. L. Jr; Dill, K. A.; Zuckermann, R. N.; Cohen, F. E. Chiral N-substituted glycines can form stable helical conformations. *Fold. Des.* **1997**, *2*, 369–375.

[12] a) Shah, N. H.; Butterfoss, G. L.; Nguyen, K.; Yoo, B.; Bonneau, R.; Rabenstein, D. L.; Kirshenbaum, K. Oligo(N-aryl glycines): A New Twist on Structured Peptoids. *J. Am. Chem. Soc.* **2008**, *130*, 16622–16632; b) De Santis, E.; Edwards, A. A.; Alexander, B. D.; Holder, S. J.; Biesse-Martin, A. S.; Nielsen, B. V.; Mistry, D.; Waters, L.; Siligardi, G.; Hussain, R.; Faure, S.; Taillefumier, C. Selective complexation of divalent cations by a cyclic α,β-peptoid hexamer: a spectroscopic and computational study. *Org. Biomol. Chem.* **2016**, *14*, 11371–11380; c) Butterfoss, G. L.; Renfrew, P. D.; Kuhlman, B.; Kirshenbaum, K.; Bonneau R. A Preliminary Survey of the Peptoid Folding Landscape. *J. Am. Chem. Soc*. **2009**, *131*, 16798−16807; d) Spencer, R. K.; Butterfoss, G. L.; Edison, J. R.; Eastwood, J. R.; Whitelam, S.; Kirshenbaum, K.; Zuckermann, R. N. Stereochemistry of polypeptoid chain configurations. *Biopolymers*, **2019**, e23266; e) Paul, B.; Butterfoss, G. L.; Boswell, M. G.; Huang, M. L.; Bonneau, R.; Wolf, C.; Kirshenbaum, K. N-Naphthyl Peptoid Foldamers Exhibiting Atropisomerism. *Org. Lett.* **2012**, *14*, 926–929. f) Baskin, M.; Panz, L.; Maayan, G. Versatile ruthenium complexes based on 2,2′-bipyridine modified peptoids. *Chem. Commun.* **2016**, *52*, 10350–10353.

[13] a) de Brevern, A. G.; Extension of the classical classification of β-turns. *Sci. Rep*. **2016**, *6*, 33191; b) Pelay-Gimeno, M.; Glas, A.; Koch, O.; Grossmann, T. N. Structure-Based Design of Inhibitors of Protein–Protein Interactions: Mimicking Peptide Binding Epitopes. *Angew. Chem., Int. Ed*. **2015**, *54*, 8896–8927; c) Nemethy G.; Printz, M. P. The γ Turn, a Possible Folded Conformation of the Polypeptide Chain. Comparison with the ß Turn. *Macromolecules*, **1972**, *5*, 755–758; d) Kaewpet, M.; Odell, B.; King, M. A.;

Banerji, B.; Schofield, C. J.; Claridge T. D. W. Synthesis and conformational analysis of cyclic analogues of inverse γ-turns. *Org. Biomol. Chem.*, **2008**, *6*, 3476–3485.

[14] The Cα−H/O=C eclipsed conformation (with formation of χ_1 dihedral angles of around ±120°, Figure 2b) pervades the previously reported structures of peptoid PPI-like helices: Stringer, J. R.; Crapster, J. A.; Guzei, I. A.; Blackwell, H. E. Extraordinarily Robust Polyproline Type I Peptoid Helices Generated via the Incorporation of α-Chiral Aromatic N-1-Naphthylethyl Side Chains. *J. Am. Chem. Soc*. **2011**, *133*, 15559−15567. See also ref. 7c and 7e.

[15] DMSO stabilizes the "crown" conformations (see: Kessler, H.; Kondor, P.; Krack, G.; Krämer, P. Conformational equilibrium in the backbone of cyclic tripeptides. *J. Am. Chem. Soc.* **1978**, *100*, 2548–2550). DMSO was therefore used as solvent for NMR spectroscopy and calculations for models **1**/**2**. In all the other studied structures chloroform was used as deuterated solvent (for NMR spectroscopy) and as implicit solvent for calculations.

[16] a) Guruprasad, K.; Rajkumar, S. β- and γ-turns in protein revisited: A new set of amino acid turns-type dependent positional preferences and potentials. *J. Biosci.*, **2000**, *25*, 143–156; b) Kahn, M.; Eguchi, M. in *Synthesis of Peptides and Peptidomimetics*; Vol. E22c, Chapter 12.2, pp. 741–758, Thieme, Stuttgard, 2004.

[17] Changing reaction conditions (PyBOP/DIPEA or EDC/HOBt/TEA) invariably yielded **8** and **9** (see SI). To the best of our knowledge this is the first time that this heterocyclic nucleus is reported in the chemical literature.

[18] Oxazolonium ions are reported as unwanted reactive species during the carbodiimide-mediated amide condensations (their intrinsic ability to enolize induces epimerization of stereogenic centers of chiral amino acid residues).

[19] Kates, S. A.; Albericio, F. (Eds.) in *Solid Phase Synthesis*: *A Practical Guide*, Marcel Dekker, Inc., New York. 2000.

[20] Formation of (*S*)-3,4,5,6-tetrahydro-3-hydroxy-1,4,5-tris((*S*)-1-phenylethyl)-1H-pyrrolo[2,3-b]pyrazine-2,7-dione (**15**) was reasonably due to autoxidation processes. Its structure was confirmed by spectroscopic and spectrometric analyses of the crystalline sample, see SI.

[21] Che, Y.; Marshall, G. L. Engineering cyclic tetrapeptides containing chimeric amino acids as preferred reverse-turn scaffolds. *J. Med. Chem.* **2006**, *49*, 111–124.

[22] Schettini, R.; Costabile, C.; Della Sala, G.; Iuliano, V.; Tedesco, C.; Izzo, I.; De Riccardis F. Cation-Induced Molecular Switching Based on Reversible Modulation of Peptoids Conformational States. *J. Org. Chem.* **2018**, *83*, 12648–12663.

[23] Shaug, J. Ring inversion in Cyclotrisarcosyl. *Acta Chem. Scand.*, **1971**, *25*, 2771–2772.

[24] Titlestad, K. Cyclic Peptides of Sarcosine. Synthesis and Conformation. *Acta Chem. Scand. B*, **1975**, *29*, 153–167.

[25] Given the overlapping of the signals and the complexity of the signal patterns it was difficult to assign the structure via one- and two-dimensional NMR spectroscopy.

[26] The structure is mentioned by Butterfoss et al. in ref. 12h, but unfortunately no structural data are provided. Thus, we decided to determine the X-ray crystal structure and report data for the first time.

[27] The relatively high value of the energy difference between the species, the massive structure of the octamer cyclopeptoid and the intrinsic slowness of conformational inversion, generate relatively complex NMR spectra (as evident in the SI).

[28] Due to their small ring size and rigidity, trimeric and tetrameric peptoids do not form discernible metal complexes in the presence of sodium ion. Maulucci, N.; Izzo, I.; Bifulco, G.; Aliberti, A.; De Cola, C.; Comegna, D.; Gaeta, C.; Napolitano, A.; Pizza, C.; Tedesco, C.; Flot, D.; De Riccardis, F. Synthesis, Structures, and Properties of Nine-, Twelve-, and Eighteen-Membered *N*-Benzyloxyethyl Cyclic α-Peptoids. *Chem. Commun.* **2008**, 3927–3929.

[29] Izzo, I.; Ianniello, G.; De Cola, C.; Nardone, B.; Erra, L.; Vaughan, G.; Tedesco, C.; De Riccardis, F. Structural Effects of Proline Substitution and Metal Binding on Hexameric Cyclic Peptoids. *Org. Lett*. **2013**, *15*, 598–601.

[30] Gorske, B. C.; Mumford, E. M.; Gerrity, C. G.; Ko, I. A Peptoid Square Helix via Synergistic Control of Backbone Dihedral Angles. *J. Am. Chem. Soc*. **2017**, *139*, 8070−8073.

[31] Dumonteil, G.; Bhattacharjee, N.; Angelici, G.; Roy, O.; Faure, S.; Jouffret, L.; Jolibois, F.; Perrin, L.; Taillefumier, C. Exploring the Conformation of Mixed Cis- Trans α,β-Oligopeptoids: A Joint Experimental and Computational Study. *J. Org. Chem.* **2018**, 83, 6382−6396.

[32] Culf, A. S.; Čuperlović-Culf, M.; Léger, D. A.; Decken, A. Small head-to-tail macrocyclic α-peptoids. *Org. Lett.* **2014**, *16*, 2780−2783.

[33] Gaussian 09, Revision A.02, Frisch, M. J.; Trucks, G. W.; Schlegel, H. B.; Scuseria, G. E.; Robb, M. A.; Cheeseman, J. R.; Scalmani, G.; Barone, V.; Mennucci, B.; Petersson, G. A.; Nakatsuji, H.; Caricato, M.; Li, X.; Hratchian, H. P.; Izmaylov, A. F.; Bloino, J.; Zheng, G.; Sonnenberg, J. L.; Hada, M.; Ehara, M.; Toyota, K.; Fukuda, R.; Hasegawa, J.; Ishida, M.; Nakajima, T.; Honda, Y.; Kitao, O.; Nakai, H.; Vreven, T.; Montgomery, J. A., Jr.; Peralta, J. E.; Ogliaro, F.; Bearpark, M.; Heyd, J. J.; Brothers, E.; N. Kudin, K.; Staroverov, V. N.; Kobayashi, R.; Normand, J.; Raghavachari, K.; Rendell, A.; Burant, J. C.; Iyengar, S. S.; Tomasi, J.; Cossi, M.; Rega, N.; Millam, J. M.; Klene, M.; Knox, J. E.; Cross, J. B.; Bakken, V.; Adamo, C.; Jaramillo, J.; Gomperts, R.; Stratmann, R. E.; Yazyev, O.; Austin, A. J.; Cammi, R.; Pomelli, C.; Ochterski, J. W.; Martin, R. L.; Morokuma, K.; Zakrzewski, V. G.; Voth, G. A.; Salvador, P.; Dannenberg, J. J.; Dapprich, S.; Daniels, A. D.; Farkas, O.; Foresman, J. B.; Ortiz, J. V.; Cioslowski, J.; Fox, D. J. Gaussian, Inc., Wallingford CT, **2009**.

[34] (a) Becke, A. Density-Functional Exchange-Energy Approximation with Correct Asymptotic Behavior. *Phys. Rev. A* **1988**, *38*, 3098–3100. (b) Perdew, J. P. Density-Functional Approximation for the Correlation Energy of the Inhomogeneous Electron Gas. *Phys. Rev. B* **1986**, *33*, 8822–8824. c) Perdew, J.

P. Erratum: Density-Functional Approximation for the Correlation Energy of the Inhomogeneous Electron Gas. *Phys. Rev. B* **1986**, *34*, 7406–7406.

[35] Schaefer, A.; Horn, H.; Ahlrichs, R. Fully Optimized Contracted Gaussian Basis Sets of Triple Zeta Valence Quality for Atoms Li to Kr. *J. Chem. Phys.* **1994**, *100*, 5829–5835.

[36] (a) Barone, V.; Cossi, M. Quantum Calculation of Molecular Energies and Energy Gradients in Solution by a Conductor Solvent Model. *J. Phys. Chem. A* **1998**, *102*, 1995–2001. (b) Tomasi, J.; Persico, M. Molecular Interactions in Solution: An Overview of Methods Based on Continuous Distributions of the Solvent. *Chem. Rev*. **1994**, *94*, 2027–2094.

[37] APEX3, SAINT, SADABS. Bruker AXS Inc., Madison, Wisconsin, USA. Bruker AXS Inc., Madison, Wisconsin, USA, **2012**.

[38] Sheldrick, G. M. A short history of SHELX. *Acta Cryst.* **2008**, *A64*, 112–122.

[39] Sheldrick, G. M. Crystal structure refinement with SHELXL. *Acta Cryst.* **2015**, *C71*, 3–8.

[40] Dolomanov, O. V.; Bourhis, L. J.; Gildea, R. J.; Howard, J. A. K.; Puschmann, H. OLEX2: a complete structure solution, refinement and analysis program. *J. Appl. Cryst.* **2009**, *42*, 339–341.